

# Motion distractors perturb saccade programming later in time than static distractors

Devin H. Kehoe<sup>a,b,c,d,\*</sup>, Lukas Schießer<sup>e</sup>, Hassaan Malik<sup>f</sup>, Mazyar Fallah<sup>a,b,c,d,f,g</sup>

<sup>a</sup> Department of Psychology, York University, Toronto, M3J 1P3, Canada

<sup>b</sup> Centre for Vision Research, York University, Toronto, M3J 1P3, Canada

<sup>c</sup> VISTA: Vision Science to Applications, York University, Toronto, M3J 1P3, Canada

<sup>d</sup> Canadian Action and Perception Network, Canada

<sup>e</sup> Institute of Cognitive Science, Universität Osnabrück, Osnabrück, 49074, Germany

<sup>f</sup> School of Kinesiology and Health Science, York University, Toronto, M3J 1P3, Canada

<sup>g</sup> College of Biological Science, University of Guelph, Guelph, N1G 2W1, Canada

## ARTICLE INFO

### Keywords:

Behavioral chronometry  
Eye movements  
Target selection  
Sensorimotor processing  
Saccade curvature  
Saccade averaging

## ABSTRACT

The mechanism that reweights oculomotor vectors based on visual features is unclear. However, the latency of oculomotor visual activations gives insight into their antecedent featural processing. We compared the oculomotor processing time course of grayscale, task-irrelevant static and motion distractors during target selection by continuously measuring a battery of human saccadic behavioral metrics as a function of time after distractor onset. The motion direction was towards or away from the target and the motion speed was fast or slow. We compared static and motion distractors and observed that both distractors elicited curved saccades and shifted endpoints at short latencies (~25 ms). After 50 ms, saccade trajectory biasing elicited by motion distractors lagged static distractor trajectory biasing by 10 ms. There were no such latency differences between distractor motion directions or motion speeds. This pattern suggests that additional processing of motion stimuli occurred prior to the propagation of visual information into the oculomotor system. We examined the interaction of distractor processing time (DPT) with two additional factors: saccadic reaction time (SRT) and saccadic amplitude. Shorter SRTs were associated with shorter DPT latencies of biased saccade trajectories. Both SRT and saccadic amplitude were associated with the magnitude of saccade trajectory biases.

## 1. Introduction

The role of the oculomotor system in saccadic target selection has been studied extensively (Basso and Wurtz, 1997, 1998; Bichot and Schall, 1999; Horwitz and Newsome, 1999, 2001; McPeck and Keller, 2002, 2004; Shen and Paré, 2007). However, the role of the oculomotor system in feature extraction and discrimination—a necessary component of target selection in the real-world—receives less attention. As such, it remains unclear whether oculomotor substrates are sufficient for feature extraction and discrimination during target selection, or alternatively, whether features are extracted and discriminated in specialized visual cortices.

Specialized visual cortical modules exhibit robust visual afferent delay times differences between them (Bodelón et al., 2007; Nowak and Bullier, 1997; Schmolesky et al., 1998). As such, one method to

investigate whether visual projections into oculomotor substrates are feature-dependent is to compare the latency of oculomotor activation elicited by features processed in different cortical modules. The dependence account would predict that oculomotor activation latencies mimic those observed in the relevant visual cortices, while the independence account would predict that oculomotor activation latencies are undifferentiated between features. Although the latency of oculomotor activation is modulated by luminance (Bell et al., 2006; Li and Basso, 2008a) and chromaticity (Hall and Colby, 2014, 2016) contrast energy, there is evidence that oculomotor activation latencies are dependent on feature-relevant visual afferent processing channels. White et al. (2009) demonstrated that visual onset burst latencies are approximately 30–35 ms faster for maximum-luminance-contrast saccade targets than for maximum-chromaticity-contrast isoluminant color targets in collicular neurons. This difference is remarkably similar to the visual afferent

\* Corresponding author. York University Faculty of Health Behavioural Science Building Room 101, 4700 Keele St., Toronto, Ontario M3J 1P3, Canada.  
E-mail address: [dhkehoe@yorku.ca](mailto:dhkehoe@yorku.ca) (D.H. Kehoe).

<https://doi.org/10.1016/j.crneur.2023.100092>

Received 25 September 2022; Received in revised form 24 May 2023; Accepted 27 May 2023

Available online 10 June 2023

2665-945X/© 2023 The Authors. Published by Elsevier B.V. This is an open access article under the CC BY-NC-ND license (<http://creativecommons.org/licenses/by-nc-nd/4.0/>).

delay time differences observed between these stimuli in the dorsal and ventral processing streams of V1 and V2.

This logic can be applied to experiments with human populations as many experimental paradigms have been developed to non-invasively infer the time course of sensory processing in the oculomotor system. These paradigms typically involve displaying an intervening visual stimulus while an impending movement is in preparation, such as saccadic (Edelman and Xu, 2009; Reingold and Stampe, 2002) or microsaccadic (Buonocore and McIntosh, 2012; Hafed and Ignashchenkova, 2013) inhibition paradigms, compelled saccades (Salinas et al., 2010; Shankar et al., 2011; Stanford et al., 2010), and double-stepping targets (Becker and Jürgens, 1979; Findlay and Harris, 1984; Ludwig et al., 2007). Similarly, Kehoe et al. (2017, 2021) recently developed a paradigm whereby subjects plan and execute a saccade to a target and we abruptly onset a peripheral distractor at some random interval after target onset. This randomizes the duration of time in which the distractor is visually present prior to the saccade. Over hundreds of trials, a rich, wide range of these time intervals are collected and a continuous variable we refer to as distractor processing time emerges. We use a battery of behavioral saccade metrics to examine saccadic perturbations as a function of distractor processing time. Specifically, we analyze saccade trajectory spatial biases, suppressed saccade initiation, and stimulus selection errors (if applicable), as each of these phenomena has a clear neurophysiological antecedent in the intermediate layers of the superior colliculus (SCi) and the frontal eye fields (FEF), two critical oculomotor substrates that determine oculomotor behavior.

Oculomotor substrates encode the direction-amplitude vectors of both eye movements (Robinson and Fuchs, 1969; Robinson, 1972) and visual stimuli (Bruce and Goldberg, 1985; Goldberg and Wurtz, 1972) as increased neural activation on orderly retinotopic maps, whereby the constituent visuomotor (VM) neurons have spatially overlapping motor and visual fields (Marino et al., 2008). The spatiotemporally weighted average of neural activation levels across the vector map determines the resultant saccadic trajectory: in the perisaccadic interval between 30 and 0 ms prior to saccade execution, increased activation at a distractor locus can curve saccade trajectories (McPeck et al., 2003; McPeck, 2006; Port and Wurtz, 2003) and shift endpoints (Glimcher and Sparks, 1972; Glimcher and Sparks, 1993) towards the distractor, while decreased activation at the distractor locus can curve saccade trajectories away from the distractor (Aizawa and Wurtz, 1998; White et al., 2012). Upon activation of a saccade vector in SCi, lateral inhibitory networks impose transient inhibition on neighboring saccade vectors (Munoz and Istvan, 1998), which manifests as lower visual onset burst magnitudes for stimulus dense displays (Basso and Wurtz, 1997, 1998) and a transient drop in saccadic likelihood after the onset of a secondary stimulus (Buonocore and McIntosh, 2012; Edelman and Xu, 2009; Reingold and Stampe, 2002).

There is considerable evidence that the latency of saccadic perturbations in humans reflects the afferent delay time of visual representations in oculomotor substrates. Visual onset burst latencies in SCi are usually ~50 ms as measured by direct physiological observation (reviewed by Boehnke and Munoz, 2008). Consistent saccadic behavior perturbation latency estimates of ~50 ms have been observed across human behavioral paradigms and metrics, such as double-stepping targets biasing saccadic endpoints (Becker and Jürgens, 1979; Findlay and Harris, 1984; Ludwig et al., 2007), luminance flashes (Reingold and Stampe, 2002) and distractor onsets (Buonocore and McIntosh, 2012; Edelman and Xu, 2009; Kehoe et al., 2021) suppressing saccadic initiation, and distractor onsets biasing saccade trajectories (Kehoe and Fallah, 2017; Kehoe et al., 2021). Previously, we observed that luminance-modulated Gabors perturb saccade trajectories approximately 20 ms faster than color-modulated Gabors (Kehoe and Fallah, 2017), consistent with visual onset burst latency differences for similar stimuli (White et al., 2009). More recently, Kehoe et al. (2021) showed that saccadic perturbation latencies were 40 ms longer for task-relevant, pseudo-alphanumeric characters as compared to task irrelevant Gabors.

This 40 ms difference is consistent with visual afferent delay time differences in early (e.g., primary visual cortex) and late (e.g., inferotemporal cortex) stages of the cortical visual processing hierarchy.

With our behavioral paradigm, we have not yet examined oculomotor activation latency differences between visual features processed in the same visual modules with visual features processed in separate visual modules using the same subjects. In the current experiment, we compared saccade perturbation latencies elicited by static, fast-motion, and slow-motion task-irrelevant distractor gratings using our behavioral paradigm. We utilized 8 and 4°/s as our fast and slow motion speeds given a classic electrophysiologically relevant boundary of 6°/s delineating fast and slow motion (ffytche et al., 1995). If motion requires additional processing over static gratings (e.g., MT vs. V1), and if the oculomotor system receives visual input after sufficient antecedent featural processing, saccade perturbation latencies should be longer for motion distractors than for static distractors. Since there are no visual processing time differences between these motion speeds (Azzopardi et al., 2003), we do not expect activation latency differences between our fast- and slow-motion distractors. We quantified saccade perturbation as saccade curvature, biased saccade endpoints (herein referred to as endpoint deviation), and a transient drop in saccadic likelihood. Additionally, we compared distractor motion towards and away from the target, as task-irrelevant motion can reflexively bias eye movement in the direction of motion (Fallah and Reynolds, 2012) and because some oculomotor cells preferentially activate for motion directed into their motor field (Horwitz and Newsome, 1999, 2001). We therefore expected a greater magnitude of saccadic trajectory perturbation for distractor motion away from the target, as distractor motion may bias the movement in the direction opposite the target and because motion away may elicit less target activation. We also split the data into upwards and downwards saccades and again compared static and motion distractors to investigate whether processing differences between static and motion distractors generalized across vertical visual hemifields. Given the strong anisotropy in the latency and magnitude of collicular visual responses (Hafed and Chen, 2016), we expect saccade perturbation latencies are shorter and perturbation magnitudes are greater in the upper visual hemifield. Finally, we extensively examined the interaction of saccadic reaction time (SRT) and saccadic amplitude on measuring saccade perturbations as a function of distractor processing time. This enabled us to disentangle executive processing (SRT) and kinematics (amplitude) from sensory processing (distractor processing time). Based on previous observations using our paradigm, we expected that SRT would affect the magnitude of saccade perturbations but not the latencies (Kehoe et al., 2021). Also, given that a subset of VM cells have open-ended motor fields in which they discharge a motor burst at increasingly longer latencies after movement initiation as saccadic amplitudes increase beyond their preferred amplitude (Munoz and Wurtz, 1995a, 1995b), we expected that saccade perturbation magnitude should be functionally related to saccade amplitude.

## 2. Methods

### 2.1. Participants

31 York University undergraduate students (16–37 years old, 4 male) participated in the experiment for course credit. Participants had normal or corrected-to-normal visual acuity and were naïve to the purpose and design of the experiment. Informed consent was obtained prior to participation. All research was approved by York University's Human Participants Review Committee.

### 2.2. Stimuli

The saccade target was a white (CIExy = [0.29, 0.30], luminance = 122.70 cd/m<sup>2</sup>) square that subtended 0.6° × 0.6° and was located 12° above or below central fixation. Distractors were sinusoidal motion



perturbations. We refer to these parameters as *onset*, *max*, and *magnitude* herein.

To estimate *onset*, we used a sliding Wilcoxon signed-rank test to determine the earliest distractor processing times at which saccade curvature and endpoint deviation were significantly different than zero for at least 10 ms. To estimate *max* and *magnitude*, we averaged the kernel regressions across subjects and computed the distractor processing time of maximum saccade curvature/endpoint deviation and the maximum saccade curvature/endpoint deviation *per se* (respectively).

These 3 parameters were estimated using the aggregated data across subjects and not on the individual subject level, making direct inferential comparisons impossible between parameters estimated in different conditions. As such, we bootstrapped the raw data  $b = 1000$  times and repeated the above analyses for each resample to estimate the sampling distribution of each parameter. We compared each parameter between distractor conditions using exhaustive pairwise two-tailed distribution tests of the independently resampled distributions. The distribution test empirically evaluates the cutoffs of a computationally approximated joint probability density function of two independent distributions (see Poe et al., 2005 for derivation and overview). For two independent distributions  $\mathbf{x} = (x_1, \dots, x_n)$  and  $\mathbf{y} = (y_1, \dots, y_m)$ , the left-tailed cumulative probability is

$$p = \frac{1}{nm} \sum_{i=1}^n \sum_{j=1}^m z_{i,j}, \text{ for } z_{i,j} = \begin{cases} 0, & \text{if } x_i \leq y_j \\ 1, & \text{otherwise} \end{cases}$$

and the two-tailed cumulative probability is  $2 \times \min\{p, 1 - p\}$ .

In a final step, we used a sliding Friedman test to determine the distractor processing times at which saccade curvature and endpoint deviation were significantly different between distractor conditions for at least 10 ms. Here, significant epochs separated by less than 5 ms were pooled together.

### 2.6.2. Saccade initiation perturbations

We used Gaussian kernel density estimation (KDE) to estimate the observed probability density of saccades as a function of distractor processing time for each subject in each distractor condition. We used LOOCV with a log-likelihood loss function to select the maximum likelihood bandwidth for each model. Next, we estimated the distractor processing time of a transient drop in saccadic likelihood, which requires some model of expected saccadic likelihood for comparison. However, there is no analytic-form for a random variable such as distractor processing time, which is the difference between two other random variables, one with multiple widely-spaced jittered peaks (DTOA) and one that is a heavily-skewed Gaussian (SRT). Therefore, we computationally generated an expectation model of saccadic likelihood for comparison with observed saccadic likelihood.

To generate our expectation model, we randomly sampled with replacement SRTs observed on baseline (i.e., distractor absent) trials pooled across participants (with  $n = 978$  trials to sample), and then independently sampled DTOAs observed on valid trials with distractor onsets. The difference of these distributions gave a bootstrapped empirical distribution of expected distractor processing times. We fit this expectation distribution with KDE using the average bandwidth across subjects in each condition.

We used a sliding Wilcoxon signed-rank test to determine the earliest distractor processing time at which observed saccade density was significantly lower than the expectation model, which we herein refer to as *onset*. We repeated the bootstrapping procedure, distribution tests, and sliding Friedman analysis discussed in the previous section.

### 2.6.3. Distractor processing time interactions with SRT and saccade amplitude

We analyzed whether the parameter estimates outlined in the previous 2 sections were consistent across the ranges of SRT and saccade amplitude observed in the data. To this end, we used Gaussian kernel

regression to estimate saccade curvature and endpoint deviation as a 2D function of distractor processing time and saccadic reaction time for each subject. We repeated this analysis for 2D functions of distractor processing time and saccade amplitude. We used LOOCV with a least squares loss function to estimate optimally predictive bandwidths for each subject. Similarly, we used Gaussian KDE to estimate saccade probability density as a 2D function of distractor processing time and SRT or distractor processing time and saccade amplitude. We used LOOCV with a log-likelihood loss function to estimate the maximum likelihood bandwidth for each subject.

At each level of SRT (range = [150 ms, 275 ms], scale = 1 ms) or saccade amplitude (range = [10°, 14°], scale = 0.025°) in the 2D functions, we repeated the 1D distractor processing time analyses outlined in the previous 2 sections. We therefore obtained parameter estimates as a function of SRT and amplitude. As before, we bootstrapped the raw data  $b = 1000$  times to generate a distribution of these parameter estimates as a function of SRT and amplitude. We used a sliding distribution test to determine the SRT or saccade amplitude values at which the 2D parameter distributions were significantly different than the omnibus parameter distributions from the preceding two sections. We used the same sliding inferential analysis conventions as above. Finally, to examine whether there was an overall linear trend of the 2D parameter estimates, we developed a computational linear regression analysis for large distributions. First, for each bootstrap, we used ordinary least squares to fit linear models of parameter estimate as a function of SRT or amplitude. Second, we computed the squared error of all 2D parameter estimates from the fitted models and unitized the variance. Third, we squared the distribution of best-fitting slopes from step 1 and unitized the variance. Last, we compared the squared/unitized distributions of model residuals and slopes from step 2 and step 3 using a one-tailed distribution test. This analysis is analogous to a non-central F-test with degrees of freedom arbitrarily close to infinity.

## 3. Results

### 3.1. Expectation model

To better illustrate the derivation of the expectation model, we show each expected (bootstrapped) distribution of distractor processing times relative to the observed distribution, split by distractor-target onset time (DTOA) condition (see Fig. 2). In panels A through D, the expected distractor processing time (DPT) distributions (DPT = DTOA – SRT; see Fig. 1B) closely resemble the SRT distribution shifted back in time by DTOA ms. The sum of these distributions gives the expectation model (see Fig. 2E). In Fig. 2, we present these data as count densities to illustrate the relative mass of saccades in each DTOA condition. In the DTOA = 200 ms condition (Fig. 2D), there is a much smaller mass of saccades relative to the remaining conditions, as many of these trials were trimmed from the data since saccades landed on target and ended the trial prior to distractor onset. Note that the same bootstrapped distribution of expected distractor processing times was used to compute the expectation model for every split of the data by distractor condition. In each condition, the expected distribution was fit using the optimal KDE bandwidth for the respective condition, thus creating the distractor-specific expectation model.

### 3.2. Distractor motion

We compared saccade curvature, endpoint deviation, and saccade density as a function of distractor processing time between static distractors and the aggregate of all motion distractors (see Fig. 3). Descriptive statistics for the bootstrapped distributions of parameters in the static and motion distractor conditions are in Table 1.

For saccade curvature (see Fig. 3A), the *onset* latency was very short (~26 ms) and did not differ between distractor conditions ( $p = .480$ ). The *max* latency was clearly differentiated between the static (100 ms)

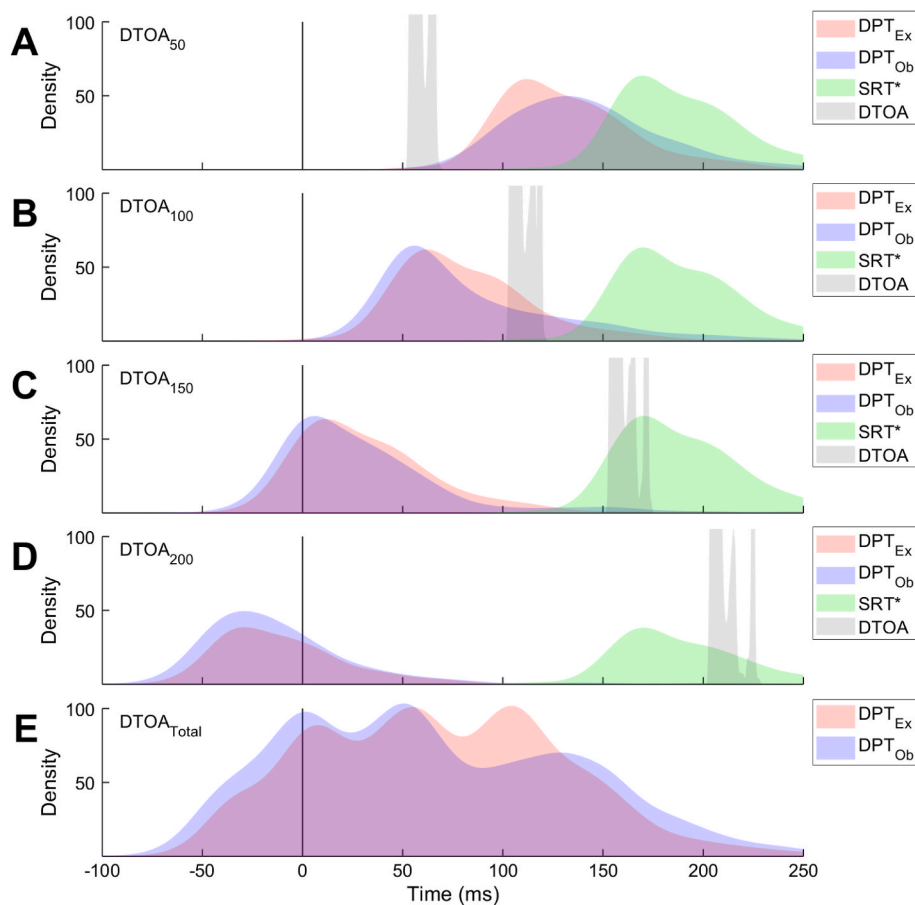


**Fig. 2.** Expected vs. observed distractor processing time (DPT) distributions split by distractor-target onset asynchrony (DTOA). Expected DPT distributions are plotted in red. Observed DPT distributions are plotted in blue. Bootstrapped SRT distributions are plotted in green. Observed DTOA distributions are plotted in gray. **A:** DTOA = 50 ms. **B:** DTOA = 100 ms. **C:** DTOA = 150 ms. **D:** DTOA = 200 ms. **E:** Aggregate of all DTOAs. (For interpretation of the references to color in this figure legend, the reader is referred to the Web version of this article.)

and motion distractors (109 ms;  $p = .001$ ), but the *magnitude* was not ( $p = .369$ ). The sliding Friedman analysis identified 2 epochs in which saccade curvature was significantly different between distractor conditions: 65–88 ms and 109–139 ms. These epochs closely corresponded to the rising and falling edges of the positively signed curvature effect.

For endpoint deviation (see Fig. 3B), the *onset* latency also had a short latency ( $\sim 30$  ms) and did not differ between distractor conditions ( $p = .853$ ). The *max* latency was  $\sim 80$  ms and was not different between conditions ( $p = .116$ ). Similarly, the *magnitude* was not different between conditions ( $p = .576$ ). Like saccade curvature, the sliding Friedman analysis identified epochs in which endpoint deviation was significantly different between distractor conditions coinciding with the rising (36–52 ms) and falling edges (101–138 ms) of the initial endpoint deviation effect.

Next, we examined the latency of saccade density falling below the expectation model (see Fig. 3C). This *onset* latency was shorter in the static condition (49 ms) than in the motion condition (62 ms;  $p = .003$ ). The sliding Friedman analysis identified two early epochs in which saccade density was different between distractor conditions:  $-3$  to 13 ms and 44–67 ms. These differences seem to reflect the fact that the static saccade density distribution is flatter in the range of 0 through 70 ms of distractor processing time as compared to the motion saccade density distribution. Beyond 70 ms, however, the two distributions are indistinguishable. This flattening effect in the static condition coincides with an increase of the width of the distribution into the negative distractor processing range as compared to motion distractors. Negative distractor processing times only arise when saccades begin after distractor onset. Since distractor onset times were identical in the static and motion distractor conditions, this increased density in the negative distractor processing range suggests increased SRTs for static distractors. Accordingly, a Wilcoxon signed-rank test confirmed that median SRT

across subjects was longer for static distractors ( $M = 200.15$  ms,  $SE = 3.50$  ms) than for motion distractors ( $M = 195.00$  ms,  $SE = 3.48$  ms) ( $p < .001$ ). It is unclear whether static distractors slowed SRT or motion distractors speeded SRTs.

### 3.3. Distractor motion direction

Next, we compared saccade curvature, endpoint deviation, and saccade density as a function of distractor processing time between static distractors, distractors with motion towards the distractor, and distractors with motion away from the target (see Fig. 4). Descriptive statistics for the bootstrapped distributions of parameters in the static, motion towards, and motion away distractor conditions are in Table 1.

For saccade curvature (see Fig. 4A), the *onset* latency was not different between distractor conditions (all  $p \geq .313$ ). The *max* latency was clearly differentiated between the static (100 ms) and motion towards distractors (110 ms;  $p < .001$ ) and motion away distractors (107 ms;  $p = .006$ ). However, there was no difference between the motion towards and motion away conditions ( $p = .278$ ). The *magnitude* was not different between conditions (all  $p \geq .328$ ). The sliding Friedman analysis identified 2 epochs in which saccade curvature was significantly different between distractor conditions: 76–88 ms and 110–141 ms.

For endpoint deviation (see Fig. 4B), the *onset* latency was not different between distractor conditions (all  $p \geq .259$ ). The *max* latency was marginally different between the static (77 ms) and motion towards distractors (84 ms;  $p = .068$ ) but was otherwise not significantly different between conditions (all  $p \geq .161$ ). The *magnitude* was not different between conditions either (all  $p \geq .110$ ). The sliding Friedman analysis identified 2 epochs in which endpoint deviation was significantly different between distractor conditions: 39–48 ms and 96–146

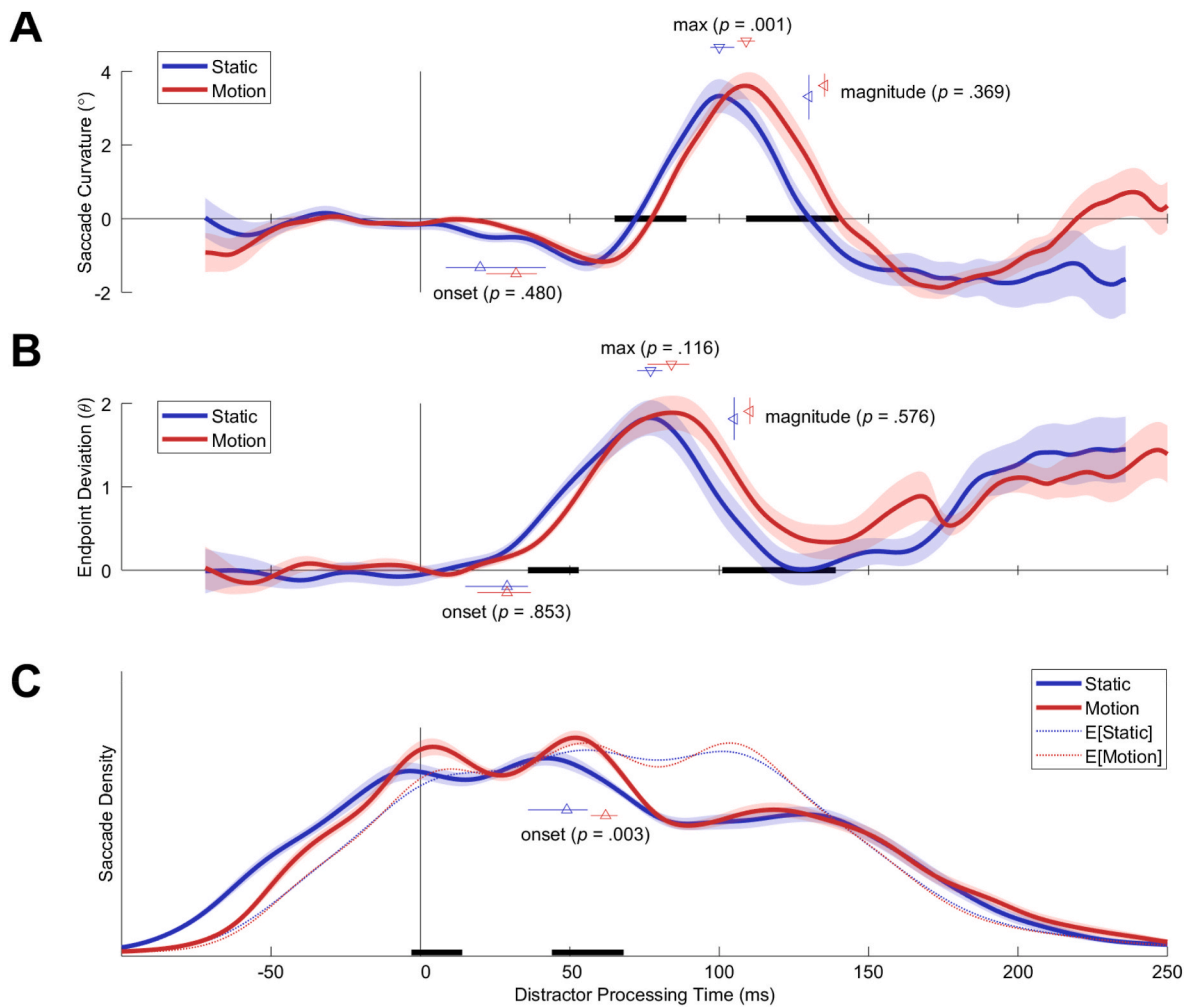


**Fig. 3.** Saccade metrics as a function of distractor processing time split by static (blue) and motion (red) distractor types. Mean saccade metrics are plotted with thick, colored lines. Standard error of the mean across subjects ( $n = 31$ ) is indicated by shading. Black lines along the abscissa in each panel indicate epochs of significant ( $p < .05$ , sliding Friedman test) differences between saccade metrics. Arrowheads indicate the estimated onset latency of saccadic perturbation ( $\blacktriangle$ ), the estimated time of maximum saccadic perturbation ( $\blacktriangledown$ ), and the magnitude of saccadic perturbation ( $\blacktriangleleft$ ). Arrowheads are color-coded to indicate distractor condition. Error bars intersecting the arrowheads indicate the bootstrapped 95% confidence interval of each point estimate.  $P$  values indicate significance (distribution test) of the difference between bootstrapped point estimates in each condition. **A:** Mean saccade curvature as a function of distractor processing time. **B:** Mean endpoint deviation as a function of distractor processing time. **C:** Mean saccade probability density as a function of distractor processing time. Dotted lines indicate expectation models. (For interpretation of the references to color in this figure legend, the reader is referred to the Web version of this article.)

ms.

The *onset* latency of lower than expectation saccade density was shorter in the static condition (49 ms) than in the motion towards (62 ms;  $p = .008$ ) and motion away (63 ms;  $p = .005$ ) conditions (see Fig. 4C). There was no difference between the motion towards and motion away conditions ( $p = .718$ ). The sliding Friedman analysis identified two epochs in which saccade density was different between distractor conditions:  $-1$  to 13 ms and 53–69 ms.

### 3.4. Distractor motion speed

We compared saccade curvature, endpoint deviation, and saccade density as a function of distractor processing time between static distractors, distractors with slow motion, and distractors with fast motion (see Fig. 5). Descriptive statistics for the bootstrapped distributions of parameters in the static, slow motion, and fast motion are in Table 1.

For saccade curvature (see Fig. 5A), the *onset* latency was not different between distractor conditions (all  $p \geq .313$ ). The *max* latency was shorter in the static (100 ms) condition than the slow motion condition (110 ms;  $p < .001$ ) and the fast motion condition (107 ms;  $p =$

.012). There was no such difference between the slow motion and fast motion conditions ( $p = .144$ ). The *magnitude* was not different between conditions (all  $p \geq .686$ ). The sliding Friedman analysis identified 2 epochs in which saccade curvature was significantly different between distractor conditions: 75–85 ms and 113–142 ms.

For endpoint deviation (see Fig. 5B), the *onset* latency was not different between distractor conditions (all  $p \geq .133$ ). The *max* latency was faster in the static condition (77 ms) than the fast motion condition (83 ms;  $p = .035$ ) but was otherwise not significantly different between conditions (all  $p \geq .247$ ). The *magnitude* was not different between conditions either (all  $p \geq .513$ ). The sliding Friedman analysis identified 3 epochs in which endpoint deviation was significantly different between distractor conditions: 38–51 ms, 96–110, and 116–130 ms.

The *onset* latency of lower than expectation saccade density was shorter in the static condition (49 ms) than in the slow motion (61 ms;  $p = .025$ ) and fast motion (64 ms;  $p = .005$ ) conditions (see Fig. 5C). There was no difference between the motion towards and motion away conditions ( $p = .423$ ). The sliding Friedman analysis identified a single epoch in which saccade density was different between distractor conditions (50–65 ms).

**Table 1**  
Descriptive statistics for bootstrapped parameter distributions in all distractor conditions.

Metric	Parameter	Distractor Condition	Median	95% CI	
				Lower	Upper
Saccade Curvature	<i>onset</i>	Static	20	8.00	41.72
		Motion	32	21.55	38.33
		Toward	37	22.33	41.71
		Away	31	23.23	38.20
		Slow	31	17.50	37.43
		Fast	36	23.00	41.97
	<i>max</i>	Static	100	96.67	104.06
		Motion	109	105.23	111.30
		Toward	110	106.11	111.94
		Away	107	103.59	111.16
		Slow	110	106.20	112.82
		Fast	107	102.65	110.44
	<i>magnitude</i>	Static	3.32	2.69	3.89
		Motion	3.62	3.31	3.94
		Toward	3.39	2.97	3.77
		Away	3.68	3.26	4.09
		Slow	3.44	3.06	3.81
		Fast	3.46	3.05	3.90
Endpoint Deviation	<i>onset</i>	Static	29	14.42	35.24
		Motion	29	18.55	36.06
		Toward	36	23.33	41.55
		Away	28	14.33	34.64
		Slow	25	15.19	35.14
		Fast	34	27.29	38.63
	<i>max</i>	Static	77	72.00	80.62
		Motion	84	75.25	89.05
		Toward	84	76.17	89.00
		Away	82	74.67	89.54
		Slow	83	73.62	89.89
		Fast	83	78.11	86.52
	<i>magnitude</i>	Static	1.81	1.56	2.07
		Motion	1.90	1.75	2.07
		Toward	1.99	1.76	2.22
		Away	1.76	1.57	1.94
		Slow	1.79	1.60	1.98
		Fast	1.89	1.69	2.08
Saccade Density	<i>onset</i>	Static	49	34.67	55.57
		Motion	62	56.50	65.40
		Toward	62	56.12	66.60
		Away	63	56.05	66.75
		Slow	61	53.11	65.05
		Fast	64	56.77	67.35

Note: 95% CI is 95% confidence interval of the bootstrapped parameter distribution. *onset* is the onset latencies saccadic perturbation. *max* is the onset latency of maximum saccadic perturbation. *magnitude* is the magnitude of maximum saccadic perturbation.

### 3.5. Visual hemifield

We compared saccade curvature, endpoint deviation, and saccade density as a function of distractor processing time between distractor type (static, motion)  $\times$  vertical visual hemifield (upper, lower) (see Fig. 6).

For saccade curvature (see Fig. 6A), the *onset* latency was not different between distractor conditions (all  $p \geq .302$ ). The *max* latency was shorter for all static distractor conditions than all motion distractor condition regardless of hemifield (all  $p \leq .033$ ). There was no hemifield differences between static ( $p = .609$ ) or motion ( $p = .831$ ) distractors. Conversely, the *magnitude* was lesser for all lower hemifield conditions than all upper hemifield distractors condition regardless of static/motion type (all  $p \leq .004$ ). There were no static/motion differences between lower ( $p = .536$ ) or upper ( $p = .339$ ) visual hemifield distractors. The sliding Friedman analysis indicated that saccade curvature was significantly different between distractor conditions across the full range of the positive saccade curvature epoch: 77–139 ms.

For endpoint deviation (see Fig. 6B), the *onset* latency of the upper

motion distractor was surprisingly longer than both lower visual hemifield distractors (all  $p \leq .026$ ). No other distractor condition differences were significant (all  $p \geq .079$ ). The *max* latency was longer for the lower motion distractor than all static distractors (all  $p \leq .040$ ). The *max* latency was shorter for the lower static distractor than all remaining distractors (all  $p \leq .032$ ). No other distractor condition differences were significant (all  $p \geq .193$ ).

The *magnitude* was different between all conditions (all  $p \leq .002$ ), except between upper static and upper motion ( $p = .442$ ). The sliding Friedman analysis indicated that endpoint deviation was significantly different between distractor conditions across the full range of the positive endpoint deviation epoch: 26–136 ms.

The *onset* latency of lower than expectation saccade density was shorter latency in the lower static condition than in both motion (all  $p \leq .003$ ) conditions (see Fig. 6C). There was no difference between any remaining distractor conditions (all  $p \geq .062$ ). The sliding Friedman analysis identified two epochs in which saccade density was different between distractor conditions: –5–10 ms and 44–68 ms.

### 3.6. Distractor processing time interaction with SRT

We analyzed whether distractor processing time parameters measured continuously as a function of SRT differed from distractor processing time parameters measured using the aggregate of all SRT values (see Fig. 7). 2D analyses were performed on the data in the motion distractor condition to maximize the amount of data. We only analyzed data within the empirical 90% confidence intervals of the distractor processing time and saccadic reaction time distributions.

We first analyzed saccade curvature as a 2D function of distractor processing time and saccadic reaction time (see Fig. 7A). The *onset* parameter was unrelated to SRT (see Fig. 7B). There was no linear trend of the *max* parameter ( $p = .282$ ; see Fig. 7C) as a function of SRT. However, the *max* parameter as a function of SRT was significantly lower than the aggregate *max* parameter in the SRT interval of 223–248 ms. There was a significant linear trend of the *magnitude* parameter as a function of SRT ( $p = .015$ ; see Fig. 7D) and *magnitude* as a function of SRT was significantly lower than the aggregate *magnitude* in the SRT interval of 239–275 ms. Note that 275 ms is the end of the SRT range in our data and that this trend may actually extend further in time.

Next, we analyzed endpoint deviation as a 2D function of distractor processing time and saccadic reaction time (see Fig. 7E). There was no linear trend of the *max* parameter ( $p = .308$ ; see Fig. 7G) as a function of SRT. There was a significant linear trend of the *onset* ( $p = .003$ ; see Fig. 7F) and the *magnitude* ( $p = .049$ ; see Fig. 7H) parameters as a function of SRT. Correspondingly, the *onset* parameter as a function of SRT was significantly higher than the aggregate *onset* parameter in the SRT interval of 234–275 ms and the *magnitude* parameter as a function of SRT was significantly lower than the aggregate *magnitude* parameter in the SRT interval of 227–275 ms.

Finally, we analyzed saccade density as a 2D function of distractor processing time and saccadic reaction time (see Fig. 7I). The LOOCV procedure correctly determined the statistical structure of the data as the 2D saccade density function was parsed into 4 disjoint distributions, one for each DTOA value. As such, we could not compare the 1D expectation model to the distractor processing time data at each level of SRT.

### 3.7. Distractor processing time interaction with amplitude

We analyzed whether distractor processing time parameters measured continuously as a function of saccade amplitude differed from distractor processing time parameters measured using the aggregate of all saccade amplitude values (see Fig. 8). 2D analyses were performed on the data in the motion distractor condition to maximize the amount of data. We only analyzed data within the empirical 90% confidence intervals of the distractor processing time and saccadic amplitude distributions.

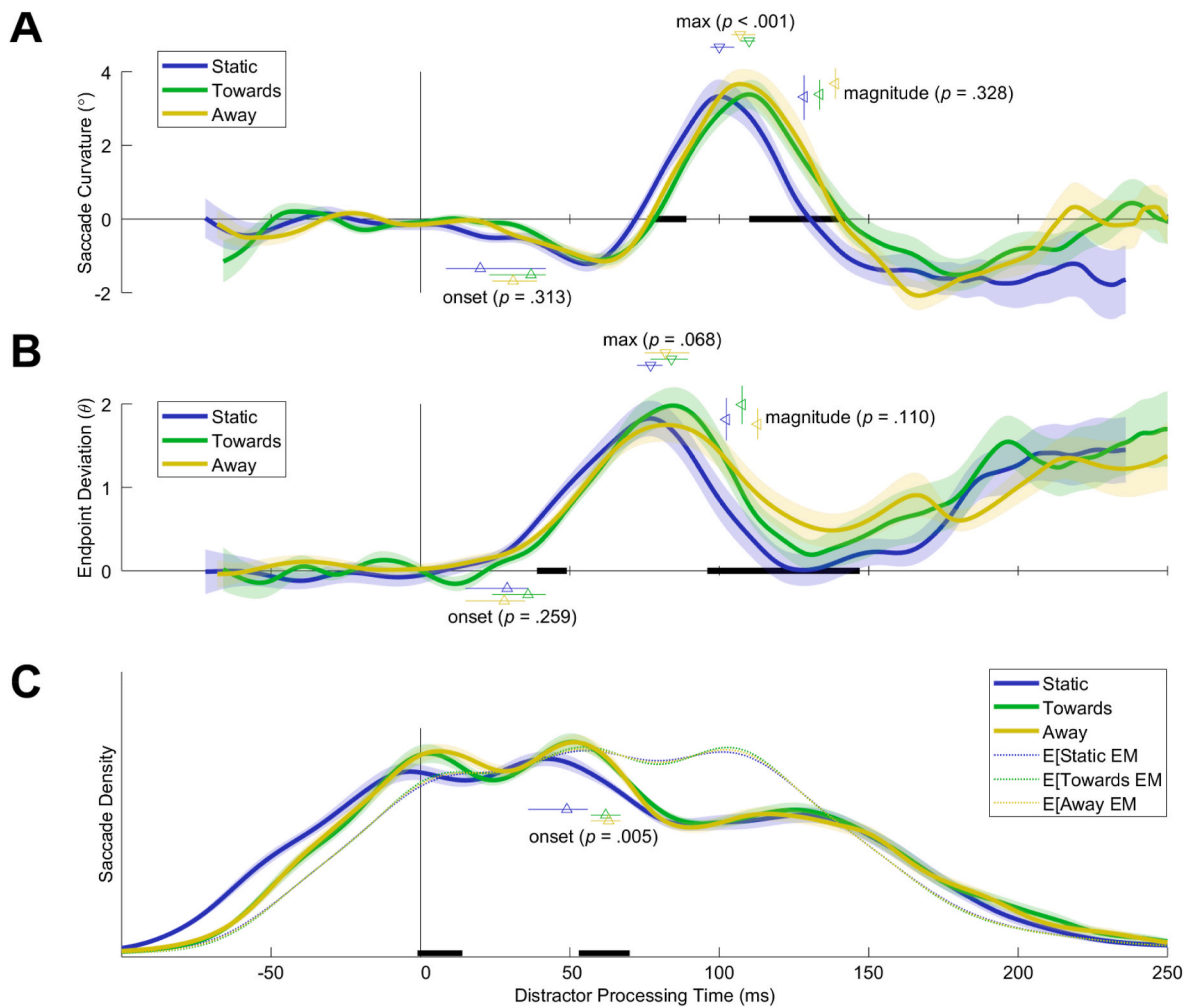


**Fig. 4.** Saccade metrics as a function of distractor processing time split by static (blue), motion towards the target (green), and motion away from the target (yellow) distractor types. Mean saccade metrics are plotted with thick, colored lines. Standard error of the mean across subjects ( $n = 31$ ) is indicated by shading. Black lines along the abscissa in each panel indicate epochs of significant ( $p < .05$ , sliding Friedman test) differences between saccade metrics. Arrowheads indicate the estimated onset latency of saccadic perturbation ( $\blacktriangle$ ), the estimated time of maximum saccadic perturbation ( $\blacktriangledown$ ), and the magnitude of saccadic perturbation ( $\blacktriangleleft$ ). Arrowheads are color-coded to indicate distractor condition. Error bars intersecting the arrowheads indicate the bootstrapped 95% confidence interval of each point estimate.  $P$  values indicate significance (distribution test) of the difference between bootstrapped point estimates in each condition. **A:** Mean saccade curvature as a function of distractor processing time. **B:** Mean endpoint deviation as a function of distractor processing time. **C:** Mean saccade probability density as a function of distractor processing time. Dotted lines indicate expectation models. (For interpretation of the references to color in this figure legend, the reader is referred to the Web version of this article.)

We first analyzed saccade curvature as a 2D function of distractor processing time and saccadic amplitude (see Fig. 8A). There was no linear trend of the *onset* ( $p = .782$ ; see Fig. 8B) or *max* ( $p = .215$ ; see Fig. 8C) parameters as a function of amplitude. There was a significant linear trend of the *magnitude* parameter as a function of amplitude ( $p = .021$ ; see Fig. 8D) and *magnitude* as a function of amplitude was significantly lower than the aggregate *magnitude* parameter in the amplitude interval of 10.0–11.4°.

Next, we analyzed endpoint deviation as a 2D function of distractor processing time and saccadic amplitude (see Fig. 8E). There was no linear trend of the *onset* ( $p = .629$ ; see Fig. 8F), *max* ( $p = .171$ ; see Fig. 8G), or *magnitude* ( $p = .061$ ; see Fig. 8H) parameters as a function of amplitude.

Finally, we analyzed saccade density as a 2D function of distractor processing time and saccadic amplitude (see Fig. 8I). There was a strong linear trend of the *onset* parameter as a function of amplitude ( $p < .001$ ; see Fig. 8J) and the *onset* parameter as a function of amplitude was significantly higher than the aggregate *onset* parameter in the amplitude interval of 10.0–11.75°.

#### 4. Discussion

We examined saccade curvature, endpoint deviation, and saccadic likelihood as a continuous function of time after the onset of task irrelevant static and motion distractors. We observed that the latency of saccade perturbations is longer for motion distractors than for static distractors. Furthermore, the motion distractors were either fast or slow and the motion direction was either towards or away from the target. We observed no differences in the latency or magnitude of saccade perturbations between distractor motion towards or away from the distractor or between fast and slow motion distractors. Finally, we analyzed how saccadic reaction time and saccade amplitude interact with saccade perturbations as a function of distractor processing time. We saw that the latency of saccade perturbations increased with SRT, the magnitude of saccade perturbations decreased with SRT, and the magnitude of saccade curvature increased with saccade amplitude.

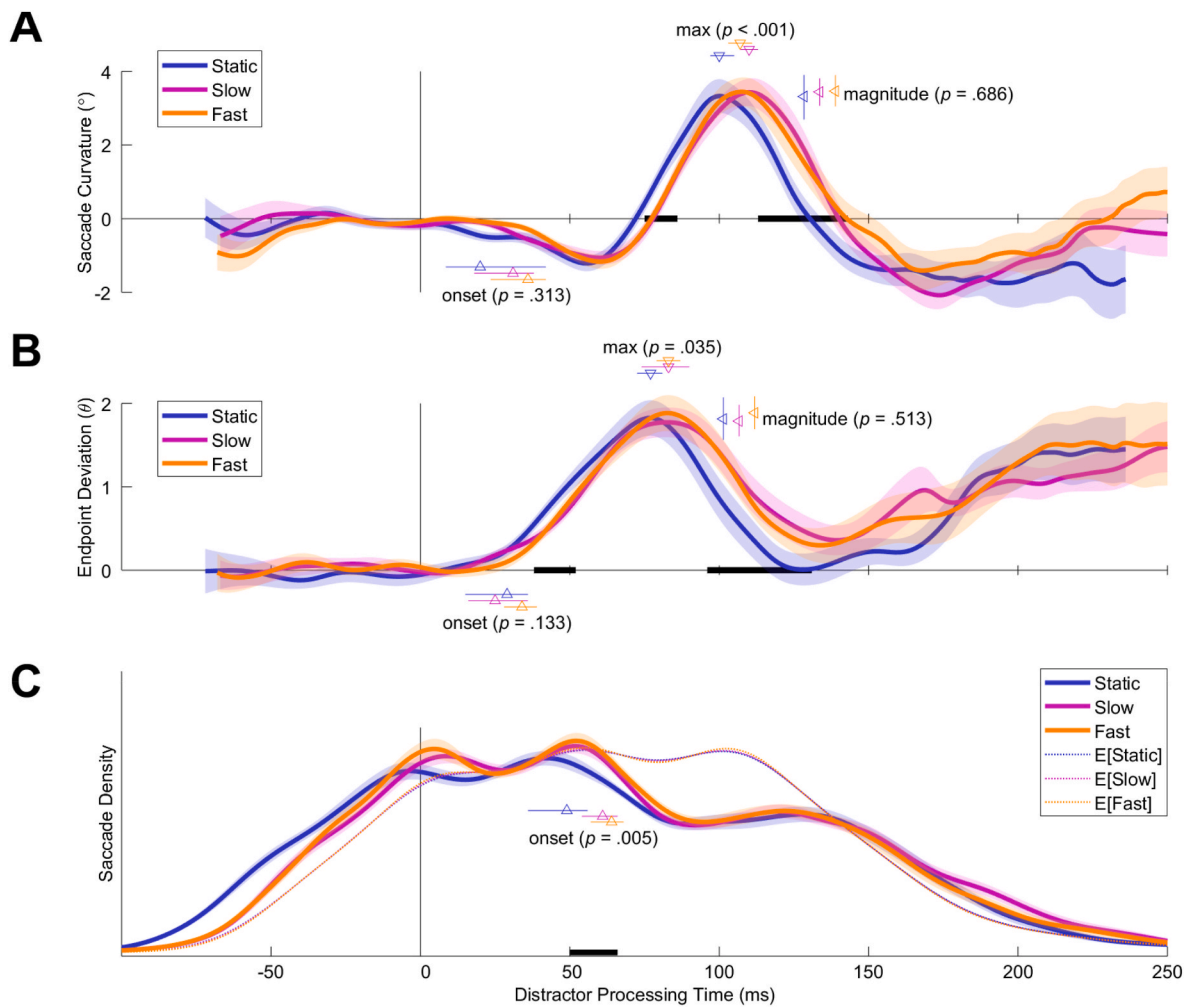


**Fig. 5.** Saccade metrics as a function of distractor processing time split by static (blue), slow motion (magenta), and fast motion (orange) distractor types. Mean saccade metrics are plotted with thick, colored lines. Standard error of the mean across subjects ( $n = 31$ ) is indicated by shading. Black lines along the abscissa in each panel indicate epochs of significant ( $p < .05$ , sliding Friedman test) differences between saccade metrics. Arrowheads indicate the estimated onset latency of saccadic perturbation ( $\blacktriangle$ ), the estimated time of maximum saccadic perturbation ( $\blacktriangledown$ ), and the magnitude of saccadic perturbation ( $\blacktriangleleft$ ). Arrowheads are color-coded to indicate distractor condition. Error bars intersecting the arrowheads indicate the bootstrapped 95% confidence interval of each point estimate.  $P$  values indicate significance (distribution test) of the difference between bootstrapped point estimates in each condition. **A:** Mean saccade curvature as a function of distractor processing time. **B:** Mean endpoint deviation as a function of distractor processing time. **C:** Mean saccade probability density as a function of distractor processing time. Dotted lines indicate expectation models. (For interpretation of the references to color in this figure legend, the reader is referred to the Web version of this article.)

#### 4.1. Distractor features

We observed that the latency of peak saccade perturbations (*max* parameters) was  $\sim 10$  ms longer for motion distractors than for static distractors. Upon onset, the first motion animation frame and static grating were indistinguishable. If visual representations of static and motion distractors were projected to the oculomotor substrates through identical channels, then no such latency difference would be expected. This latency difference is therefore consistent with our hypothesis that visual stimulus representations are projected into oculomotor substrates from the relevant cortical visual modules specialized for processing the constituent visual features characterizing the stimuli.

Middle temporal (MT) and medial superior temporal (MST) cortices process complex motion, such as the current motion grating distractor, by spatiotemporally summing downstream motion components encoded in V1, such as the current static grating distractor (Movshon et al., 1985; Movshon and Newsome, 1996; Zeki, 1974). MT and MST are thus situated higher in the cortical visual hierarchy (Maunsell and Van Essen, 1983) with a visual afferent delay time that is  $\sim 10$  ms longer than V1 (Schmolesky et al., 1998). Furthermore, processing in MT and MST is

necessary for motion perception (Bisley and Pasternak, 2000; Britten et al., 1996; Rudolph and Pasternak, 1999; Salzman et al., 1990, 1992) and certain motor behaviors like pursuit eye movements (Dürsteler et al., 1987; Dürsteler and Wurtz, 1988; Komatsu and Wurtz, 1989). Given the direct connection between V1 and MT/MST (Maunsell and Van Essen, 1983), applying the 10 ms rule-of-thumb (Nowak and Bullier, 1997), one expects a 10 ms visual afferent delay latency difference between cells in these areas on average. Since V1 is sufficient for processing the static grating, and since MT is necessary for processing the motion grating, we reason that the 10 ms latency difference we observed between static and motion distractors reflects oculomotor activation originating from different levels in the cortical processing hierarchy. Although we are unable to ascertain this speculation directly with the current behavioral methodology, this difference cannot be accounted for by other factors such as luminance contrast energy since our distractors were identical in all aspects besides motion energy. Consistent with our account of V1 and MT separately driving visual representations in oculomotor substrates, there are direct connections between V1 and superior colliculus (SC) (Fries, 1984; Lock et al., 2003), MT and SC (Maunsell and Van Essen, 1983), and MT and FEF (Schall et al., 1995).

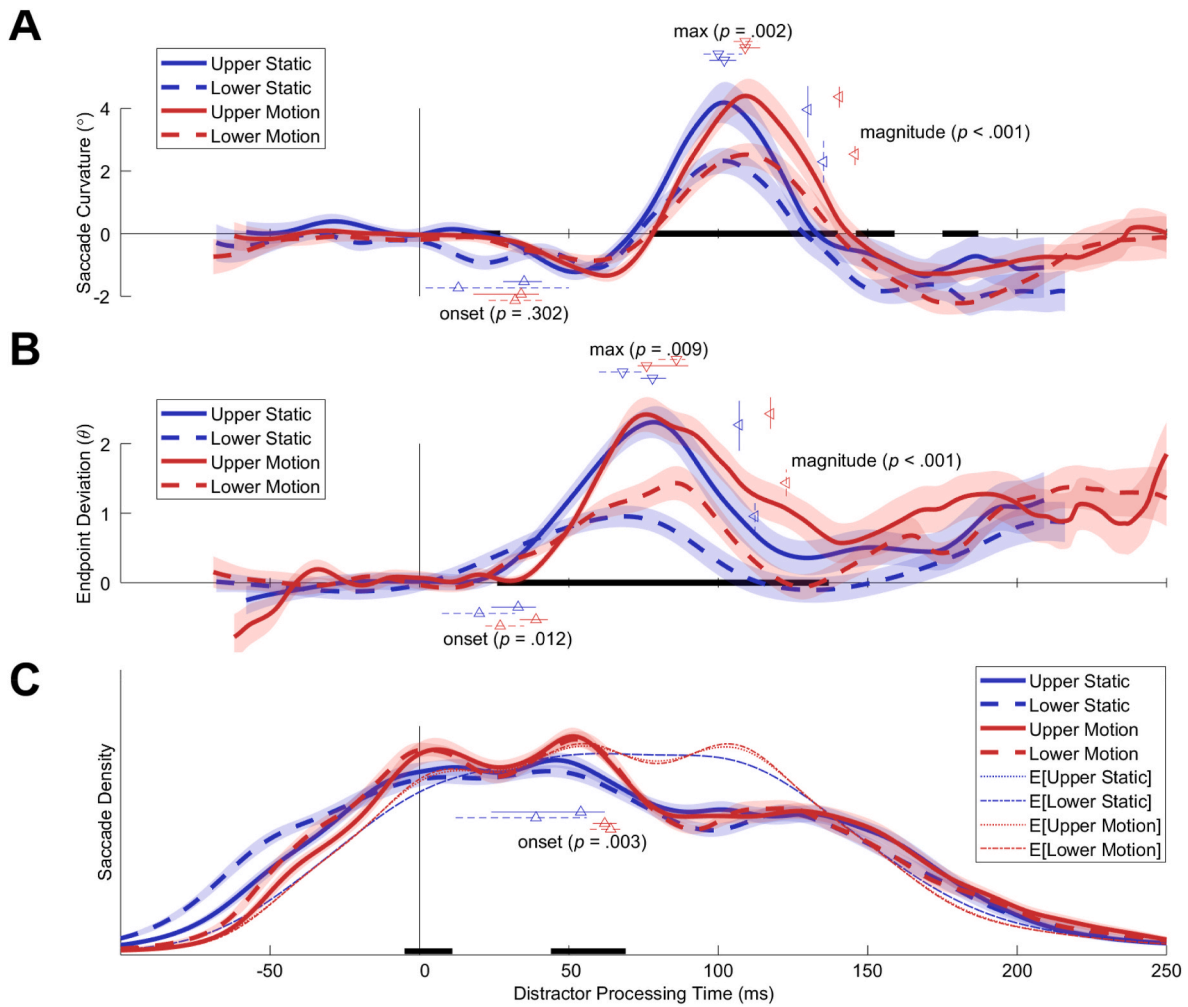


**Fig. 6.** Saccade metrics as a function of distractor processing time split by distractor type (static, motion)  $\times$  vertical visual hemifield (upper, lower). Static is plotted in blue. Motion is plotted in red. Upward saccades are plotted with solid lines. Downward saccades are plotted with broken lines. Mean saccade metrics are plotted with thick, colored lines. Standard error of the mean across subjects ( $n = 31$ ) is indicated by shading. Black lines along the abscissa in each panel indicate epochs of significant ( $p < .05$ , sliding Friedman test) differences between saccade metrics. Arrowheads indicate the estimated onset latency of saccadic perturbation ( $\blacktriangle$ ), the estimated time of maximum saccadic perturbation ( $\blacktriangledown$ ), and the magnitude of saccadic perturbation ( $\blacktriangleleft$ ). Arrowheads are color-coded to indicate distractor condition. Error bars intersecting the arrowheads indicate the bootstrapped 95% confidence interval of each point estimate.  $P$  values indicate significance (distribution test) of the difference between bootstrapped point estimates in each condition. **A:** Mean saccade curvature as a function of distractor processing time. **B:** Mean endpoint deviation as a function of distractor processing time. **C:** Mean saccade probability density as a function of distractor processing time. Dotted lines indicate expectation models for upwards saccades. Alternating dashed/dotted lines indicate expectation models for downward saccades. (For interpretation of the references to color in this figure legend, the reader is referred to the Web version of this article.)

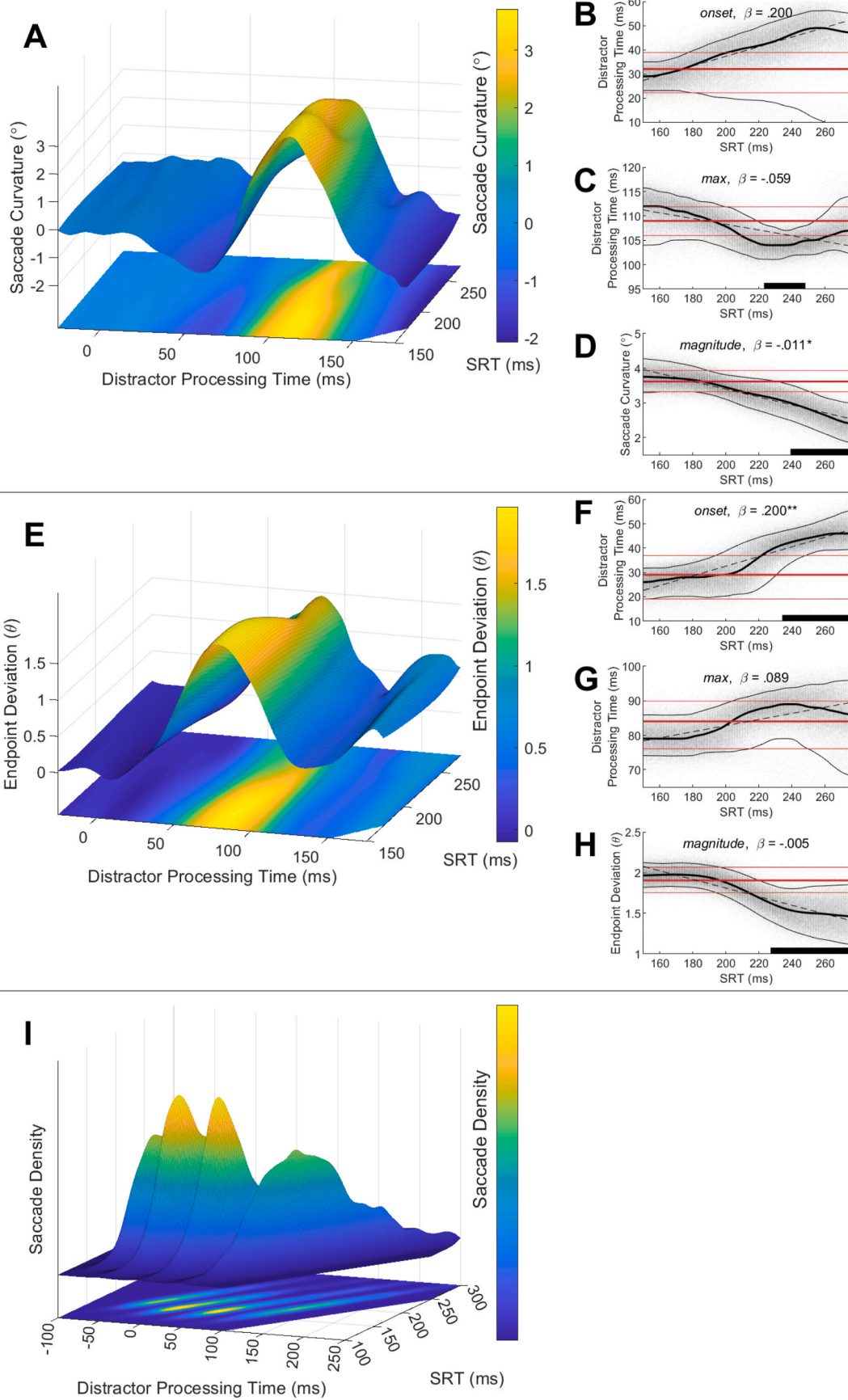
To corroborate our speculation, future behavioral experiments could examine if these same latency differences manifest for other types of stimuli that also show strong processing ties to areas V1 and MT. For example, random white noise elicits strong activation in V1 (e.g., Pack et al., 2006), while random dot fields elicit strong activation in area MT (Albright, 1984). Like the current stimuli, these stimuli are advantageous as equalizing their contrast energy and spatial locality is trivial.

White et al. (2009) showed that visual burst onset latencies in SCi cells are  $\sim 35$  ms later for maximum-chromaticity-contrast isoluminant color patches than for maximum-luminance-contrast patches. More recent work has shown that vision is trichromatically encoded in SC (Hall and Colby, 2014, 2016).

However, since visual representations in SC are completely extinguished following ablation of striatal and extrastriatal cortices (Schiller et al., 1974), color information in SC must be mediated through the retinogeniculocortical pathway. The work of White et al. therefore suggests that the visual representations encoded by SCi cells were driven separately by the magno- and parvocellular processing streams in early cortex, as these processing streams bear similar visual afferent delay

differences between them (Schmolesky et al., 1998) and because isoluminant color patches would be nearly invisible to the magnocellular pathway (Livingstone and Hubel, 1987, 1988). However, this result does not imply cortical gating *per se*, as these stimuli were simply projected along parallel pathways with inherently different conduction latencies. In contrast, our data do suggest cortical gating, as our stimuli would very likely be projected through the same processing stream. That is, the latency differences we saw can only be explained by a delay within the magnocellular processing stream, as our grayscale stimuli would elicit very weak activation in the parvocellular processing stream where only 10% of cells are responsive to broadband stimulation (Livingstone and Hubel, 1987, 1988).

We observed no difference between the latencies of saccade trajectory perturbation onset (*onset* parameters) for static and motion distractors. These parameters indicate the earliest evidence of distractor-based spatial biasing of the saccade. For endpoint deviation and saccade curvature, these latencies were both extremely short ( $\sim 25$  ms) and equal across all distractor features. At such low latencies, this must reflect direct retinotectal projections and precludes the first frame being



(caption on next page)

**Fig. 7.** Saccade metrics as a function of distractor processing time and saccadic reaction time (SRT) in the motion distractor condition. **Left panels:** Mean (across subjects,  $n = 31$ ) saccade metrics as a function of distractor processing time and SRT plotted as a 3D manifold above a 2D heatmap with a colorbar to indicate scaling. **Right subpanels:** Distractor processing time parameter estimates as a function of SRT. Black dots indicate parameter estimates at each level of SRT across  $b = 1000$  bootstrapped resamples. Thick black line indicates median of bootstrapped distributions as a function of SRT. Thin black lines indicate empirical 95% confidence intervals of bootstrapped distributions as a function of SRT. Dashed black line indicates mean linear model of parameter estimates as a function of SRT fit to each bootstrapped distribution. Text labels indicate parameter type and the mean slope ( $\beta$ ) across linear models fit to each bootstrapped distribution. Asterisks indicate significance of a one-tailed distribution test between squared, unitized slope distribution and squared, unitized model residual distribution ( $*p < .05$ ,  $**p < .01$ ,  $***p < .001$ ). Thick red line indicates median of constant 1D distribution of parameter estimates in the motion distractor condition. Thin red lines indicate empirical 95% confidence interval of constant 1D distribution of parameter estimates in the motion distractor condition. Black rectangles along abscissa indicate the SRT intervals in which the distribution of parameter estimates as a function of SRT was significantly different than the constant 1D distribution of parameter estimates ( $p < .05$ ; sliding distribution test). **A:** Mean saccade curvature as a function of distractor processing time and SRT. **B:** Saccade curvature *onset* parameter estimate as a function of SRT. **C:** Saccade curvature *max* parameter estimate as a function of SRT. **D:** Saccade curvature *magnitude* parameter estimate as a function of SRT. **E:** Mean endpoint deviation as a function of distractor processing time and SRT. **F:** Endpoint deviation *onset* parameter estimate as a function of SRT. **G:** Endpoint deviation *max* parameter estimate as a function of SRT. **H:** Endpoint deviation *magnitude* parameter estimate as a function of SRT. **I:** Mean saccade density as a function of distractor processing time and SRT. (For interpretation of the references to color in this figure legend, the reader is referred to the Web version of this article.)

processed in V1 (Schiller and Malpeli, 1977). The earliest evidence of saccade trajectory perturbation as a function of distractor processing time diverging between static and motion distractors was after  $\sim 50$  ms (i.e., 36 ms for endpoint deviation and 65 ms for saccade curvature). Qualitatively, it appeared as though the motion and static distractor processing time functions were identical in the first 50 ms, then at distractor processing times greater than 50 ms, the motion distractor processing time function was shifted behind the static function by 10 ms. Consistent with this, the drop in saccadic likelihood for static distractors occurred at 50 ms, while for motion distractors, this drop occurred at 60 ms.

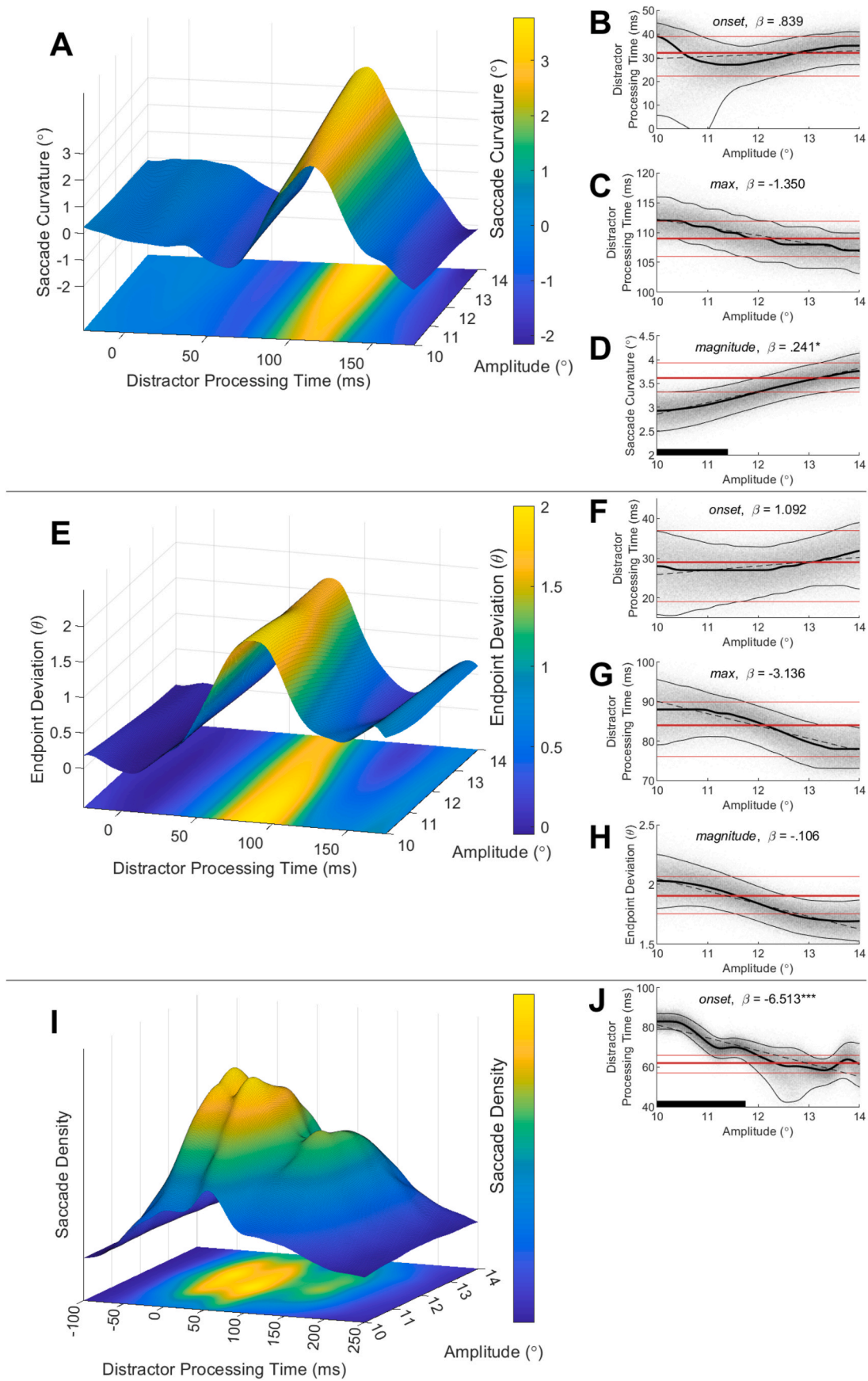
These observations suggest that visual information projected into the oculomotor substrates was cascading: first, a feature-invariant retinotectal signal indicated the location of newly acquired potential saccade targets. Second, a cortically-gated signal carried the featural information about the potential saccade targets. One alternative explanation is that this pattern of results was due to the motion animation delivering luminance transients upon every frame, whereby each new motion animation frame would elicit a rapid retinotectal swell of oculomotor activation bypassing cortex altogether. However, this cannot be the case. First, using our 85 Hz CRT to render a 40 fps animation, the first animation frame is repeated at the 11.8 and 23.5 ms refresh cycles. The second frame is finally delivered on the 35.3 ms refresh cycle. If 25 ms is the minimum retinotectal conduction time as we saw, then the second animation frame at  $\sim 35$  ms is insufficient to elicit the divergence at 50 ms. Second, this account predicts that the motion distractor processing time function should grow monotonically. However, there were no magnitude differences (*max* parameters) between the static and motion distractor processing time functions. Third, the luminance transient between animation frames should be more intense for the fast motion stimulus than the slow motion stimulus, which predicts a latency or magnitude difference between fast and slow motion distractors. However, we observed no such differences (discussed in more detail below). Given these reasons, the more plausible explanation is that the second motion animation frame engaged motion processing cortical areas that provided much stronger inputs to the oculomotor substrates and/or gated V1 visual projections to oculomotor substrates. Future investigations could test this reasoning by repeating this experiment using a higher refresh rate.

The lack of saccade perturbation latency or magnitude differences between distractor motion towards and away from the target was surprising, as large-field visual motion (Kawano and Miles, 1986; Miles et al., 1986) and small motion patches (Fallah and Reynolds, 2012) can reflexively elicit pursuit eye movements in the direction of the task-irrelevant motion stimulus. Since directional biasing of saccades and pursuit eye movements can be elicited by microstimulation from within the same oculomotor (Krauzlis and Miles, 1998; Yan et al., 2001) and visual (Groh et al., 1997) substrates, we expected that our motion distractors would also elicit reflexive directional biasing of saccades as with pursuit. If so, saccades would show increased trajectory

perturbations towards the distractor for distractor motion directed away from the target, which we did not observe. There are at least two explanations for this: first, reflexive ocular following responses are observed immediately after the execution of saccades terminating in the motion field (Fallah and Reynolds, 2012; Kawano and Miles, 1986; Miles et al., 1986), and therefore, likely arise from motion introducing spatial error signals during post-saccadic retinal stabilization processing. As saccades on our task passed through empty space and terminated on stationary targets, we would not expect dynamic spatial error signals during saccade execution or post-saccade at the saccade termination loci. Future iterations of the task could require observers to saccade through or onto a motion field to test this possibility. Second, perhaps small motion patches may only bias eye movement vectors in the context of competing motion information. Competing motion signals are encoded in MT and MST as a vector-weighted average of the motion directions on short post-stimulus time scales (Groh et al., 1997; Recanzone and Wurtz, 1999, 2000). MT and MST are critical for resolving motion-based competition during oculomotor processing (Dürsteler et al., 1987; Dürsteler and Wurtz, 1988; Komatsu and Wurtz, 1989). However, since the current target did not elicit motion competition, perhaps the oculomotor system did not utilize the distractor motion information to reweight the distractor visual representation during target selection on this task. A simple test of this speculation is to repeat this task with motion targets.

A subpopulation of cells in superior colliculus exhibits inherent motion direction sensitivities whereby they discharge higher activation for motion directed into their motor field (Horwitz and Newsome, 1999, 2001). As such, we expected that distractor motion towards the target would elicit higher target activation than distractor motion away from the target. This would bias a vector-weighted average computation in favor of the target for distractor motion towards the target. In such a case, the distractor motion away condition should elicit higher saccade perturbations than the motion towards condition; however, we did not observe this. It could be that the 30% of motion selective cells in the population (Horwitz and Newsome, 2001) which would drive this effect constitute too few of the cells encoding the stimuli to significantly bias the vector average computation.

The current experiment was the first within subjects comparison of features processed in the same cortical modules to features processed in different cortical modules using our behavioral paradigm. Cortical area MT processes fast and slow motion stimuli with no apparent visual afferent delay time differences as a function of motion strength (Azzopardi et al., 2003). As such, comparing the saccade perturbation latencies of fast and slow motion distractor types provided a complimentary test of our hypothesis that visual representations are projected into the oculomotor substrates from relevant cortical modules. As these stimuli are processed in the same cortical module, we did not expect saccadic perturbation latency difference between them, consistent with our results. Additionally, contrasting this observation with the 10 ms difference between motion and static gratings illustrates that our



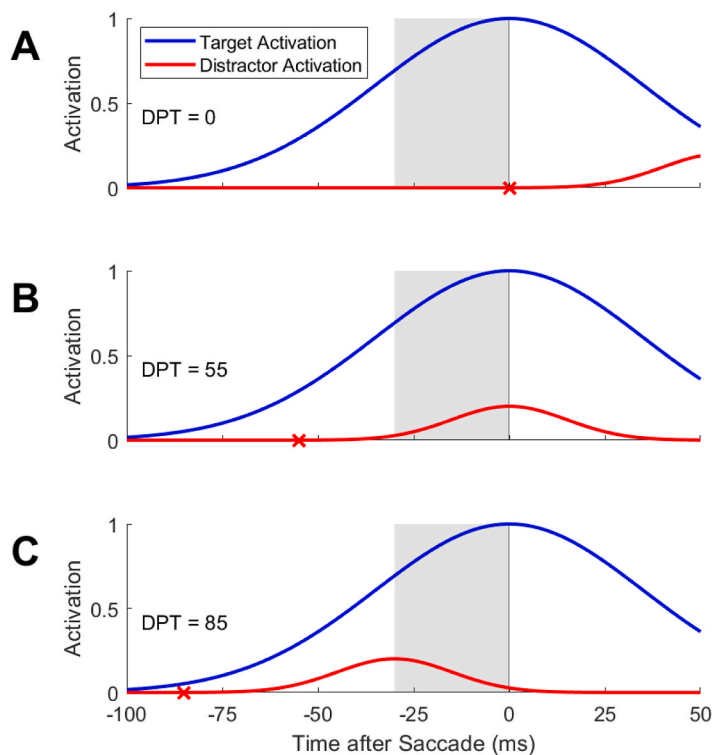
(caption on next page)

**Fig. 8.** Saccade metrics as a function of distractor processing time and saccade amplitude in the motion distractor condition. **Left panels:** Mean (across subjects,  $n = 31$ ) saccade metrics as a function of distractor processing time and saccade amplitude plotted as a 3D manifold above a 2D heatmap with a colorbar to indicate scaling. **Right subpanels:** Distractor processing time parameter estimates as a function of saccade amplitude. Black dots indicate parameter estimates at each level of saccade amplitude across  $b = 1000$  bootstrapped resamples. Thick black line indicates median of bootstrapped distributions as a function of saccade amplitude. Thin black lines indicate empirical 95% confidence intervals of bootstrapped distributions as a function of saccade amplitude. Dashed black line indicates mean linear model of parameter estimates as a function of saccade amplitude fit to each bootstrapped distribution. Text labels indicate parameter type and the mean slope ( $\beta$ ) across linear models fit to each bootstrapped distribution. Asterisks indicates significance of a one-tailed distribution test between squared, unitized slope distribution and squared, unitized model residual distribution ( $*p < .05$ ,  $**p < .01$ ,  $***p < .001$ ). Thick red line indicates median of constant 1D distribution of parameter estimates in the motion distractor condition. Thin red lines indicate empirical 95% confidence interval of constant 1D distribution of parameter estimates in the motion distractor condition. Black rectangles along abscissa indicate the saccade amplitude intervals in which the distribution of parameter estimates as a function of saccade amplitude was significantly different than the constant 1D distribution of parameter estimates ( $p < .05$ ; sliding distribution test). **A:** Mean saccade curvature as a function of distractor processing time and saccade amplitude. **B:** Saccade curvature *onset* parameter estimate as a function of saccade amplitude. **C:** Saccade curvature *max* parameter estimate as a function of saccade amplitude. **D:** Saccade curvature *magnitude* parameter estimate as a function of saccade amplitude. **E:** Mean endpoint deviation as a function of distractor processing time and saccade amplitude. **F:** Endpoint deviation *onset* parameter estimate as a function of saccade amplitude. **G:** Endpoint deviation *max* parameter estimate as a function of saccade amplitude. **H:** Endpoint deviation *magnitude* parameter estimate as a function of saccade amplitude. **I:** Mean saccade density as a function of distractor processing time and saccade amplitude. **J:** Saccade density *onset* parameter estimate as a function of saccade amplitude. (For interpretation of the references to color in this figure legend, the reader is referred to the Web version of this article.)

latency effects are related to featural complexity and not simply differences between motion strength. One possibility is that our fast and slow motion speeds were not sufficiently differentiated to elicit a true difference (see ffychte et al., 1995). Although this account is discredited by Azzopardi et al. (2003), it could nevertheless be investigated in future iterations of this experiment using markedly different motion speeds (e.g.,  $5^\circ/s$  vs.  $25^\circ/s$ ).

#### 4.2. Non-invasive computational modelling of target selection

We observed clear evidence of an initial epoch of negative curvature



preceding the subsequent epoch of positive curvature. We also observed this phenomenon in the previous two investigations of saccade perturbations as a function of distractor processing time and either dismissed this effect (Kehoe and Fallah, 2017) or interpreted it as top-down inhibition (Kehoe et al., 2021). However, the vector-weighted average model of Port and Wurtz (2003) offers a more plausible explanation: saccade trajectories are computed as the instantaneous vector-weighted average of the target and distractor vectors weighted by the activation at the target and distractor loci on the oculomotor map. This computation occurs between approximately 30 to 0 ms prior to saccade execution (McPeck et al., 2003; McPeck, 2006; Port and Wurtz, 2003; White et al.,

critical epoch. Minimal averaging should occur in the early portion of the saccade, while maximum averaging should occur in the latter portion of the saccade. This is consistent with observation as, at this DPT, saccades were initially straight but then curved towards the distractor in the latter portion. **C:** Distractor onset occurs 85 ms before saccade initiation (distractor processing time = 85). The visual onset burst is aligned with the lower portion of the critical epoch. Maximum averaging should occur in the initial portion of the saccade, but minimal averaging should occur in the latter portion of the saccade. This is consistent with observation as, at this DPT, the saccade is initially directed in between the target and distractor, but angles back towards the target in the latter portion. (For interpretation of the references to color in this figure legend, the reader is referred to the Web version of this article.)

**Fig. 9.** Theoretical and empirical saccadic vector-weighted averaging. **Left panels:** Hypothetical neural activation as a function of time before saccade initiation for oculomotor cells encoding the target (blue) or the distractor (red). Gray shaded region indicates the critical epoch between 30 and 0 ms prior to saccade initiation. Saccade trajectories are determined by the vector-weighted average of the target and distractor activation functions in the critical epoch. Red “x” indicates the distractor onset time. Text label indicates corresponding distractor processing time (DPT). Distractor activation functions had a 30 ms initial phase as reported elsewhere (McPeck and Keller, 2002) and a lead time of 25 ms after distractor onset as was observed in the current experiment. **Right panels:** Example displays with target (square), fixation (“+”), distractor (grating), and observed saccade trajectories (gray and black traces). Gray traces are average saccade trajectories for each subject at the respective distractor processing time ( $\pm 5$  ms) indicated by the text label in each row. Trajectories were angularly scaled by  $10^\circ$  for illustrative purposes (e.g., a saccade trajectory angled  $45^\circ$  towards the distractor was actually observed as only  $4.5^\circ$ ). Black traces are the average saccade trajectories across subjects. **A:** Distractor onset occurs at the time of saccade initiation (distractor processing time = 0). The visual onset burst elicited by the distractor is well outside the critical epoch and no averaging should occur. This is consistent with observation as saccades were straight at this DPT. **B:** Distractor onset occurs 55 ms before saccade initiation (distractor processing time = 55). The visual onset burst is aligned with the upper portion of the

2012). As can be seen in Fig. 9B, when distractor processing time begins to exceed 0, the distractor visual onset burst sweeps into the upper bound of the critical epoch. This distractor competition only affects the late portion of the saccade programming, so the saccade is initially straight but then veers towards the distractor in the latter portion. As such, the saccade is curved and the endpoint is biased towards the distractor. However, given our conceptualization of saccade curvature, saccades with this shape are negatively signed, as the deviations are directed away from the distractor with respect to a straight line connecting the beginning and end of the saccade. As can be seen in Fig. 9C, when distractor processing time increases further, the distractor visual onset burst eventually begins to align with the lower bound of the critical epoch. Therefore, the initial portion of the saccade is heavily biased towards the distractor, while the latter portion of the saccade is less averaged and directed straight towards the target. When this occurs, we see positively signed saccade curvature as these initial deviations are directed towards the distractor with respect to a straight line connecting the beginning and end of the saccade. Interestingly, this computation also presupposes that saccade deviations directed away from the distractor with respect to a straight line between fixation and the target would require a negative contribution from the distractor, such as inhibition at the distractor locus (see Aizawa and Wurtz, 1998; White et al., 2012). Testing various inhibitory mechanisms as inputs into the vector average model would provide insight into the nature of saccade deviations away from distractors, as we plan to do in future investigations.

As in a previous investigation of saccade perturbations as a function of distractor processing time (Kehoe et al., 2021), we corroborated our saccade trajectory perturbation metrics with an additional metric: saccade initiation perturbation, that is, a drop in saccade likelihood relative to an expectation model. Drops in saccade density have been observed ~60 ms after flashes of light (Reingold and Stampe, 2002) or irrelevant distractor onsets (Bunocore and McIntosh, 2012). This drop in saccadic likelihood may be related to rapid lateral inhibition in SC (Munoz and Istvan, 1998), as a similar drop in microsaccade rates is observed after the onset of a stimulus (Engbert and Kliegl, 2003; Hafed and Ignashchenkova, 2013; Rolfs et al., 2008). However, in the current experiment, we observed that the latency of this drop in saccadic likelihood was ~10 ms longer for motion stimuli than for static stimuli. This observation provides further validation of our saccade trajectory perturbation metrics and corroborates our account that visual input into the oculomotor system is cortically-gated on the basis of features, even when the features are task irrelevant.

We split the data into upwards and downwards saccades and repeated our analysis of static and motion distractors. We observed that the magnitude of saccadic trajectory perturbations was much stronger in the vertical hemifield than the lower hemifield, as expected since visual activations are much stronger in the upper visual hemifield (Hafed and Chen, 2016). For saccade curvature and saccadic likelihood, the overall pattern of latency results generalized across the two vertical hemifields: the motion activation lagged behind the static activation by approximately ~10 ms regardless of hemifield. For endpoint deviation, the results were less clear. We surprisingly saw that the estimated onset latency of endpoint deviation for upper motion distractors was slower than both lower distractors. However, visual activation latencies should be faster in the upper visual field Hafed and Chen, 2016, which suggests this is likely an artefact.

#### 4.3. Saccadic reaction time and amplitude

Previous behavioral studies examining the time-course of saccade perturbations (McSorley et al., 2006; Mulckhuysen et al., 2009) have not disentangled the role of executive processing (SRT) from sensory processing (distractor processing time). Here, we examined the interaction of distractor processing time and SRT and observed that the qualitative pattern of distractor processing time results is stable across the observed

range of SRT, but with certain quantitative differences. First, the magnitude of peak saccade trajectory perturbations as a function of distractor processing time (*max* parameter) monotonically decreased as a function of SRT. In fact, both trajectory perturbation metrics, saccade curvature and endpoint deviation, showed a nearly 50% peak perturbation magnitude reduction between the shortest (150 ms) and longest (275 ms) SRTs. This is consistent with the results from our recent experiment investigating the distractor processing time and SRT interaction elicited by markedly different stimuli: task-relevant, complex objects (Kehoe et al., 2021). This therefore demonstrates that this effect is robust across stimulus categories. Second, the initial onset latency of saccade trajectory perturbation as a function of distractor processing time (*onset* parameter) showed a monotonic increase as a function of SRT whereby at the shortest SRTs, the onset latency of saccade trajectory perturbations was merely 20 ms, and at the longest SRTs, it had increased to 50 ms.

Our results suggest that the magnitude and latency of the visual onset responses encoding distractors were gradually attenuated as a function of SRT. This implicates the role of executive processing in gating sensory input into the oculomotor system. The voluntary control of saccades is largely mediated by the cortico-nigral-tecal pathway, whereby executive cortices modulate basal ganglian activity and the substantia nigra pars reticulata of the basal ganglia (SNr) imposes tonic GABAergic inhibition on the superior colliculus (reviewed by Hikosaka et al., 2000). This circuit controls the sensitivity of VM cells in SC to sensory stimulation: GABA antagonist injections in SC produce spontaneous, irrepressible saccades into empty regions of space (Hikosaka and Wurtz, 1985a), while GABA agonist injections in SC produce misdirected, hypometric, long latency, low-velocity saccades and decreased saccadic likelihood (Aizawa and Wurtz, 1998; Hikosaka and Wurtz, 1985a; McPeck and Keller, 2004). These deficits are replicated by pharmacologically deactivating (Hikosaka and Wurtz, 1985b) and microstimulating (Basso and Liu, 2007; Liu and Basso, 2008b) SNr (respectively). The sensitivity of SC cells to sensory stimulation is directly related to SRTs as observed in express saccades, whereby visual onset responses themselves reach motor threshold and elicit extremely short latency saccades (Dorris et al., 1997; Marino et al., 2015). This mechanism provides a plausible explanation of the current interaction of SRT and distractor processing time. Perhaps on certain trials the oculomotor system was visually desensitized via tonic inhibition to minimize the competitive influence of the distractor and thus facilitate task performance, which incidentally increased SRT. We suspect that this desensitization would increase over the course of the experiment, as we observed previously that saccade perturbation magnitudes gradually decreased throughout the course of a similar experiment (Kehoe et al., 2021).

We analyzed the interaction of distractor processing time and saccadic amplitude, as saccadic amplitude is indicative of target motor activation independently of distractor visual activation. We observed that peak saccade curvature (*magnitude* parameter) strongly increased as a function of saccadic amplitude. This effect is expected from an open-ended movement field encoding scheme as seen in approximately one third of collicular neurons: saccades of equal or lesser amplitude than the cell's preferred amplitude elicit a motor burst that reaches peak excitability at the time of movement initiation, while for saccades greater than the cell's preferred amplitude, the motor burst reaches peak excitability at increasingly longer latencies after movement initiation (Munoz and Wurtz, 1995a, 1995b). Critically, for such cells encoding the target direction, saccades with a longer-than-preferred amplitude would elicit a motor burst outside of the perisaccadic interval, the interval between 30 and 0 ms prior to saccade initiation when vector-weighted averaging occurs (McPeck et al., 2003; McPeck, 2006; Port and Wurtz, 2003; White et al., 2012). Longer-than-preferred amplitude saccades would therefore diminish the target-encoding cells' contribution to the vector-weighted average computation and saccadic spatial biasing towards the distractor should increase, as observed.

We also observed that the onset latency of an abrupt drop in saccadic likelihood (*onset* parameter) strongly decreased with saccadic amplitude. This effect suggests that less lead time of a visual distractor is required for cancelling a longer saccade than for a shorter saccade. Our distractor processing time variable is equal to the distractor lead time prior to saccade onset. As such, the distractor processing time latency of an abrupt drop in saccadic likelihood can be interpreted as the minimum lead time necessary to inhibit an impending saccade. Saccades can be effectively canceled at any point midflight (Robinson and Fuchs, 1969, Robinson, 1972). Since longer saccades extend longer in time, there is a longer effective window for cancelling them.

## 5. Conclusions

Oculomotor planning and motion processing are inextricably linked (Dürsteler et al., 1987; Dürsteler and Wurtz, 1988; Komatsu and Wurtz, 1989). We utilized our human behavioral paradigm (Kehoe and Fallah, 2017; Kehoe et al., 2021) to show that during target selection, motion information is encoded by the oculomotor system after a 10 ms delay as compared to static stimuli, even though both stimulus types were task irrelevant. We suggest that this delay therefore reflects an inherent visual encoding property of the oculomotor system: visual representations are cortically gated to accommodate sufficient featural analysis. This gives insight into the process by which visual representations on oculomotor maps are feature-weighted to facilitate accurate target selection of behaviorally relevant stimuli (Bichot and Schall, 1999; Horwitz and Newsome, 1999, 2001; McPeck and Keller, 2002; Shen and Paré, 2007).

## Author contribution

D.H.K. designed research and drafted manuscript, analyzed data, prepared figures. L.S. analyzed data. H.M. performed research. M.F. designed research and drafted manuscript, approved of final draft

## Declaration of competing interest

The authors declare that they have no known competing financial interests or personal relationships that could have appeared to influence the work reported in this paper

## Data availability

Data will be made available on request.

## Acknowledgements

We would like to thank Anuj Dogra for her help collecting data. This work was supported by an NSERC Discovery Grant to M.F. (RGPIN-2016-05296) and an NSERC PGS-D scholarship to D.H.K.

## Appendix A. Supplementary data

Supplementary data to this article can be found online at <https://doi.org/10.1016/j.crneur.2023.100092>.

## References

- Aizawa, H., Wurtz, R.H., 1998. Reversible inactivation of monkey superior colliculus. I. Curvature of saccadic trajectory. *J. Neurophysiol.* 79, 2082–2096.
- Albright, T.D., 1984. Direction and orientation selectivity of neurons in visual area MT of the macaque. *J. Neurophysiol.* 52, 1106–1130.
- Azzopardi, P., Fallah, M., Gross, C.G., Rodman, H.R., 2003. Response latencies of neurons in visual areas MT and MST of monkeys with striate cortex lesions. *Neuropsychologia* 41, 1738–1756.
- Basso, M.A., Liu, P., 2007. Context-dependent effects of substantia nigra stimulation on eye movements. *J. Neurophysiol.* 97, 4129–4142.
- Basso, M.A., Wurtz, R.H., 1997. Modulation of neuronal activity by target uncertainty. *Nature* 389, 66–69.

- Basso, M.A., Wurtz, R.H., 1998. Modulation of neuronal activity in superior colliculus by changes in target probability. *J. Neurosci.* 18, 7519–7534.
- Becker, W., Jürgens, R., 1979. An analysis of the saccadic system by means of double step stimuli. *Vis. Res.* 19, 967–983.
- Bell, A.H., Meredith, M.A., Van Opstal, A.J., Munoz, D.P., 2006. Stimulus intensity modifies saccadic reaction time and visual response latency in the superior colliculus. *Exp. Brain Res.* 174, 53–59.
- Bichot, N.P., Schall, J.D., 1999. Effects of similarity and history on neural mechanisms of visual selection. *Nat. Neurosci.* 2, 549–554.
- Bisley, J.W., Pasternak, T., 2000. The multiple roles of visual cortical areas MT/MST in remembering the direction of visual motion. *Cerebr. Cortex* 10, 1053–1065.
- Bodelón, C., Fallah, M., Reynolds, J.H., 2007. Temporal resolution for the perception of features and conjunctions. *J. Neurosci.* 27, 725–730.
- Boehne, S.E., Munoz, D.P., 2008. On the importance of the transient visual response in the superior colliculus. *Curr. Opin. Neurobiol.* 18, 544–551.
- Britten, K.H., Newsome, W.T., Shadlen, M.N., Celebri, S., Movshon, J.A., 1996. A relationship between behavioral choice and the visual responses of neurons in macaque MT. *Vis. Neurosci.* 13, 87–100.
- Bruce, C.J., Goldberg, M.E., 1985. Primate frontal eye fields. I. Single neurons discharging before saccades. *J. Neurophysiol.* 53, 603–635.
- Buonocore, A., McIntosh, R.D., 2012. Modulation of saccadic inhibition by distractor size and location. *Vis. Res.* 69, 32–41.
- Dorris, M.C., Paré, M., Munoz, D.P., 1997. Neuronal activity in monkey superior colliculus related to the initiation of saccadic eye movements. *J. Neurosci.* 17, 8566–8579.
- Dürsteler, M.R., Wurtz, R.H., Newsome, W.T., 1987. Directional pursuit deficits following lesions of the foveal representation within the superior temporal sulcus of the macaque monkey. *J. Neurophysiol.* 57, 1262–1287.
- Dürsteler, M.R., Wurtz, R.H., 1988. Pursuit and optokinetic deficits following chemical lesions of cortical areas MT and MST. *J. Neurophysiol.* 60, 940–965.
- Edelman, J.A., Xu, K.Z., 2009. Inhibition of voluntary saccadic eye movement commands by abrupt visual onsets. *J. Neurophysiol.* 101, 1222–1234.
- Engbert, R., Kliegl, R., 2003. Microsaccades uncover the orientation of covert attention. *Vis. Res.* 43, 1035–1045.
- Fallah, M., Reynolds, J.H., 2012. Contrast dependence of smooth pursuit eye movements following a saccade to superimposed targets. *PLoS One* 7, e37888.
- Findlay, J.M., Harris, L.R., 1984. In: Gale, A.G., Johnson, F. (Eds.), *Small saccades to double-stepped targets moving in two dimensions, Theoretical and Applied Aspects of Eye Movement Research*. North-Holland/Elsevier Science, Amsterdam, pp. 71–78.
- Fries, W., 1984. Cortical projections to the superior colliculus in the macaque monkey: a retrograde study using horseradish peroxidase. *J. Comp. Neurol.* 230, 55–76.
- ffytche, D.H., Guy, C.N., Zeki, S., 1995. The parallel visual motion inputs into areas V1 and V5 of human cerebral cortex. *Brain* 118, 1375–1394.
- Glimcher, P.W., Sparks, D.L., 1993. Effects of low-frequency stimulation of the superior colliculus on spontaneous and visually guided saccades. *J. Neurophysiol.* 69, 953–964.
- Goldberg, M.E., Wurtz, R.H., 1972. Activity of superior colliculus in behaving monkey. I. Visual receptive fields of single neurons. *J. Neurophysiol.* 35, 542–559.
- Groh, J.M., Born, R.T., Newsome, W.T., 1997. How is a sensory map read out? Effects of microstimulation in visual area MT on saccades and smooth pursuit eye movements. *J. Neurosci.* 17, 4312–4330.
- Hafed, Z.M., Chen, C.Y., 2016. Sharper, stronger, faster upper visual field representation in primate superior colliculus. *Curr. Biol.* 26, 1647–1658.
- Hafed, Z.M., Ignashchenkova, A., 2013. On the dissociation between microsaccade rate and direction after peripheral cues: microsaccadic inhibition revisited. *J. Neurosci.* 33, 16220–16235.
- Hall, N.J., Colby, C.L., 2016. Express saccades and superior colliculus responses are sensitive to short-wavelength cone contrast. *Proc. Natl. Acad. Sci. U. S. A.* 113, 6743–6748.
- Hall, N.J., Colby, C.L., 2014. S-cone visual stimuli activate superior colliculus neurons in old world monkeys: implications for understanding blindsight. *J. Cognit. Neurosci.* 26, 1234–1256.
- Hikosaka, O., Takikawa, Y., Kawagoe, R., 2000. Role of the basal ganglia in the control of purposive saccadic eye movements. *Physiol. Rev.* 80, 953–978.
- Hikosaka, O., Wurtz, R.H., 1985a. Modification of saccadic eye movements by GABA-related substances. I. Effect of muscimol and bicuculline in monkey superior colliculus. *J. Neurophysiol.* 53, 266–291.
- Hikosaka, O., Wurtz, R.H., 1985b. Modification of saccadic eye movements by GABA-related substances. II. Effects of muscimol in monkey substantia nigra pars reticulata. *J. Neurophysiol.* 53, 292–308.
- Horwitz, G.D., Newsome, W.T., 1999. Separate signals for target selection and movement specification in the superior colliculus. *Science* 284, 1158–1161.
- Horwitz, G.D., Newsome, W.T., 2001. Target selection for saccadic eye movements: direction-selective visual responses in the superior colliculus. *J. Neurophysiol.* 86, 2527–2542.
- Kawano, K., Miles, F.A., 1986. Short-latency ocular following responses of monkey. II. Dependence on a prior saccadic eye movement. *J. Neurophysiol.* 56, 1355–1380.
- Kehoe, D.H., Fallah, M., 2017. Rapid accumulation of inhibition accounts for saccades curved away from distractors. *J. Neurophysiol.* 118, 832–844.
- Kehoe, D.H., Lewis, J., Fallah, M., 2021. Oculomotor target selection is mediated by complex objects. *J. Neurophysiol.* 126, 845–863.
- Komatsu, H., Wurtz, R.H., 1989. Modulation of pursuit eye movements by stimulation of cortical areas MT and MST. *J. Neurophysiol.* 62, 31–47.
- Krauzlis, R.J., Miles, F.A., 1998. Role of the oculomotor vermis in generating pursuit and saccades: effects of microstimulation. *J. Neurophysiol.* 80, 2046–2062.

- Li, X., Basso, M.A., 2008a. Preparing to move increases the sensitivity of superior colliculus neurons. *J. Neurosci.* 28, 4561–4577.
- Liu, P., Basso, M.A., 2008b. Substantia nigra stimulation influences monkey superior colliculus neuronal activity bilaterally. *J. Neurophysiol.* 100, 1098–1112.
- Livingstone, M.S., Hubel, D.H., 1987. Psychophysical evidence for separate channels for the perception of form, color, movement, and depth. *J. Neurosci.* 7, 3416–3468.
- Livingstone, M.S., Hubel, D.H., 1988. Segregation of form, color, movement, and depth: anatomy, physiology, and perception. *Science* 240, 740–749.
- Lock, T.M., Baizer, J.S., Bender, D.B., 2003. Distribution of corticotectal cells in macaque. *Exp. Brain Res.* 151, 455–470.
- Ludwig, C.J., Mildinhall, J.W., Gilchrist, I.D., 2007. A population coding account for systematic variation in saccadic dead time. *J. Neurophysiol.* 97, 795–805.
- Marino, R.A., Levy, R., Munoz, D.P., 2015. Linking express saccade occurrence to stimulus properties and sensorimotor integration in the superior colliculus. *J. Neurophysiol.* 114, 879–892.
- Marino, R.A., Rodgers, C.K., Levy, R., Munoz, D.P., 2008. Spatial relationships of visuomotor transformations in the superior colliculus map. *J. Neurophysiol.* 100, 2564–2576.
- Maunsell, J.H.R., Van Essen, D.C., 1983. The connections of the middle temporal visual area (MT) and their relationship to a cortical hierarchy in the macaque monkey. *J. Neurosci.* 3, 2563–2586.
- McPeck, R.M., Han, J.H., Keller, E.L., 2003. Competition between saccade goals in the superior colliculus produces saccade curvature. *J. Neurophysiol.* 89, 2577–2590.
- McPeck, R.M., Keller, E.L., 2004. Deficits in saccade target selection after inactivation of superior colliculus. *Nat. Neurosci.* 7, 757–763.
- McPeck, R.M., Keller, E.L., 2002. Saccade target selection in the superior colliculus during a visual search task. *J. Neurophysiol.* 88, 2019–2034.
- McPeck, R.M., 2006. Incomplete suppression of distractor-related activity in the frontal eye field results in curved saccades. *J. Neurophysiol.* 96, 2699–2711.
- McSorley, E., Haggard, P., Walker, R., 2006. Time course of oculomotor inhibition revealed by saccade trajectory modulation. *J. Neurophysiol.* 96, 1420–1424.
- Miles, F.A., Kawano, K., Optican, L.M., 1986. Short-latency ocular following responses of monkey. I. Dependence on temporospatial properties of visual input. *J. Neurophysiol.* 56, 1321–1354.
- Movshon, J.A., Adelson, E.H., Gizzi, M.S., Newsome, W.T., 1985. In: Chagas, C., Gattass, R., Gross, C. C. (Eds.), *The analysis of moving visual patterns, Pattern Recognition Mechanisms*. Vatican Press, Rome, pp. 117–151.
- Movshon, J.A., Newsome, W.T., 1996. Visual response properties of striate cortical neurons projecting to area MT in macaque monkeys. *J. Neurosci.* 16, 7733–7741.
- Mulckhuyse, M., Van der Stigchel, S., Theeuwes, J., 2009. Early and late modulation of saccade deviations by target distractor similarity. *J. Neurophysiol.* 102, 1451–1458.
- Munoz, D.P., Istvan, P.J., 1998. Lateral inhibitory interactions in the intermediate layers of the monkey superior colliculus. *J. Neurophysiol.* 79, 1193–1209.
- Munoz, D.P., Wurtz, R.H., 1995a. Saccade-related activity in monkey superior colliculus. I. Characteristics of burst and buildup cells. *J. Neurophysiol.* 73, 2313–2333.
- Munoz, D.P., Wurtz, R.H., 1995b. Saccade-related activity in monkey superior colliculus. II. Spread of activity during saccades. *J. Neurophysiol.* 73, 2334–2348.
- Nowak, L.G., Bullier, J., 1997. In: Rockland, K.S., Kaas, J.H., Peters, A. (Eds.), *The timing of information transfer in the visual system, Cerebral Cortex: Extrastriate Cortex in Primates*. Plenum Press, New York, pp. 205–241.
- Pack, C.C., Conway, B.R., Born, R.T., Livingstone, M.S., 2006. Spatiotemporal structure of nonlinear subunits in macaque visual cortex. *J. Neurosci.* 26, 893–907.
- Poe, G.L., Giraud, K.L., Loomis, J.B., 2005. Computational methods for measuring the difference of empirical distributions. *Am. J. Agric. Econ.* 87, 353–365.
- Port, N.L., Wurtz, R.H., 2003. Sequential activity of simultaneously recorded neurons in the superior colliculus during curved saccades. *J. Neurophysiol.* 90, 1887–1903.
- Recanzone, G.H., Wurtz, R.H., 2000. Effects of attention on MT and MST neuronal activity during pursuit initiation. *J. Neurophysiol.* 83, 777–790.
- Recanzone, G.H., Wurtz, R.H., 1999. Shift in smooth pursuit initiation and MT and MST neuronal activity under different stimulus conditions. *J. Neurophysiol.* 82, 1710–1727.
- Reingold, E.M., Stampe, D.M., 2002. Saccadic inhibition in voluntary and reflexive saccades. *J. Cognit. Neurosci.* 14, 371–388.
- Robinson, D.A., Fuchs, A.F., 1969. Eye movements evoked by stimulation of frontal eye fields. *J. Neurophysiol.* 32, 637–648.
- Robinson, D.A., 1972. Eye movements evoked by collicular stimulation in the alert monkey. *Vis. Res.* 12, 1795–1808.
- Rofls, M., Kliegl, R., Engbert, R., 2008. Toward a model of microsaccade generation: the case of microsaccadic inhibition. *J. Vis.* 8, 1–23.
- Rudolph, K., Pasternak, T., 1999. Transient and permanent deficits in motion perception after lesions of cortical areas MT and MST in the macaque monkey. *Cerebr. Cortex* 9, 90–100.
- Salinas, E., Shankar, S., Costello, M.G., Zhu, D., Stanford, T.R., 2010. Waiting is the hardest part: comparison of two computational strategies for performing a compelled-response task. *Front. Comput. Neurosci.* 4 (1–17).
- Salzman, C.D., Britten, K.H., Newsome, W.T., 1990. Cortical microstimulation influences perceptual judgements of motion direction. *Nature* 346, 174–177.
- Salzman, C.D., Murasugi, C.M., Britten, K.H., Newsome, W.T., 1992. Microstimulation in visual area MT: effects on direction discrimination performance. *J. Neurosci.* 12, 2331–2355.
- Schall, J.D., Morel, A., King, D.J., Bullier, J., 1995. Topography of visual cortex connections with frontal eye field in macaque: convergence and segregation of processing streams. *J. Neurosci.* 15, 4464–4487.
- Schiller, P.H., Malpeli, J.G., 1977. Properties and tectal projections of monkey retinal ganglion cells. *J. Neurophysiol.* 40, 428–445.
- Schiller, P.H., Stryker, M., Cyander, M., Berman, N., 1974. Response characteristics of single cells in the monkey superior colliculus following ablation or cooling of visual cortex. *J. Neurophysiol.* 37, 181–194.
- Schmolesky, M.T., Wang, Y., Hanes, D.P., Thompson, K.G., Leutgeb, S., Schall, J.D., Veenthal, G., 1998. Signal timing across the macaque visual system. *J. Neurophysiol.* 79, 3272–3278.
- Shankar, S., Massoglia, D.P., Zhu, D., Costello, M.G., Stanford, T.R., Salinas, E., 2011. Tracking the temporal evolution of a perceptual judgment using a compelled-response task. *J. Neurosci.* 31, 8406–8421.
- Shen, K., Paré, M., 2007. Neuronal activity in superior colliculus signals both stimulus identity and saccade goals during visual conjunction search. *J. Vis.* 7, 15–15.
- Stanford, T.R., Shankar, S., Massoglia, D.P., Costello, M.G., Salinas, E., 2010. Perceptual decision making in less than 30 milliseconds. *Nat. Neurosci.* 13, 379–385.
- White, B.J., Boehnke, S.E., Marino, R.A., Itti, L., Munoz, D.P., 2009. Color-related signals in the primate superior colliculus. *J. Neurosci.* 29, 12159–12166.
- White, B.J., Theeuwes, J., Munoz, D.P., 2012. Interaction between visual- and goal-related neuronal signals on the trajectories of saccadic eye movements. *J. Cognit. Neurosci.* 24, 707–717.
- Yan, Y.J., Cui, D.M., Lynch, J.C., 2001. Overlap of saccadic and pursuit eye movement systems in the brain stem reticular formation. *J. Neurophysiol.* 86, 3056–3060.
- Zeki, S.M., 1974. Functional organization of a visual area in the posterior bank of the superior temporal sulcus of the rhesus monkey. *J. Physiol.* 236, 549–573.

## Glossary

*SRT*: saccadic reaction time

*V1*: visual area 1

*V2*: visual area 2

*SCi*: intermediate layers of the superior colliculus

*FEF*: frontal eye fields

*VM*: visuomotor

*MT*: middle temporal area

*DTOA*: distractor-target onset asynchrony

*DPT*: distractor processing time

*LOOCV*: leave-one-out cross validation

*KDE*: kernel density estimation

*MST*: medial superior temporal area

*SC*: superior colliculus

*SNr*: substantia nigra pars reticulata